PHYSICAL REVIEW B VOLUME 52, NUMBER 23 15 DECEMBER 1995-I

Properties of intrinsic point defects in silicon determined by zinc diffusion experiments under nonequilibrium conditions

H. Bracht, N.A. Stolwijk, and H. Mehrer
Institut für Metallforschung Universität Münster, Wilhelm-Klemm-Strasse 10, D-48149 Münster, Germany
(Received 31 May 1995)

The present paper deals with self- and foreign-atom diffusion processes in Si. We focus on the foreign-atom Zn whose diffusion behavior is shown to be influenced by intrinsic point defects like Si self-interstitials (I) and vacancies (V). Diffusion experiments with Zn in dislocation-free Si were carried out between 1208 and 870 °C applying a special method to perform isothermal diffusion anneals as short as a few seconds. Concentration-depth profiles measured with the help of spreading-resistance analysis are completely described by simultaneous diffusion via the kickout and dissociative mechanism. The evolution of Zn diffusion with time is characterized by short-, intermediate-, and long-time diffusion regimes. Profiles belonging to the long-time regime are suitable to extract transport capacities of intrinsic defects given by the product of thermal equilibrium concentration and diffusion coefficient. Zn profiles after intermediate diffusion times are shown to be sensitive to the prevailing thermal equilibrium concentration of Si self-interstitials. Results are presented for the thermal equilibrium concentrations of self-interstitials and vacancies as well as their transport properties. From the temperature dependence of these quantities the formation and migration enthalpy of I and V are obtained. These data are compared to previous experimental results as well as theoretical calculations.

I. INTRODUCTION

The investigation of diffusion processes in solids is basic to the understanding of the microscopic diffusion mechanisms and the behavior of, e.g., involved intrinsic point defects. Information about intrinsic point defects in solids is generally gained from self-diffusion,[1] positron annihilation,[2] and differential dilatometry[3] (Simmons-Balluffi experiments). However, positron annihilation[4,5] and Simmons-Balluffi experiments[6] carried out in the case of Si yield no reliable results, since the concentration of intrinsic point defects is expected to be much lower than in metals due to the strong covalent binding. Whereas in closed packed metals vacancies (V) are the dominating intrinsic point defects, in the open structure of the Si lattice also self-interstitials (I) play a crucial role. Despite the circumstance that I and V are hardly detectable it is generally accepted that in Si both self-interstitials and vacancies have to be taken into account in order to understand the diffusion behavior of the shallow dopants like, e.g., phosphorus, boron, and antimony under oxidizing or nonoxidizing surface conditions.[7] Reliable data about thermodynamic and transport properties of I and V like the free enthalpy of migration ($G^m_{I,V}$) and formation ($G^f_{I,V}$) are basic for controlling crystal growth processes as well as dopant diffusion in Si and therefore for the fabrication of electronic devices. Since nowadays many processing steps are necessary for a new device, data concerning the properties of I and V are technologically important for process simulators which have to be optimized in order to minimize time consuming experiments, thereby enhancing the economy of the new product.

The present paper shows how the properties of intrinsic point defects in Si can be determined on the basis of foreign-atom diffusion experiments under nonequilibrium conditions. First a brief survey over self- and foreign-atom diffusion in Si is given in Sec. II. Then the electrical and diffusion behavior of the foreign atom Zn in Si is treated in Sec. III in detail. The mathematical formulation of the kick-out diffusion mechanism is presented in Sec. IV and predictions based on this mechanism are deduced. The validity of the kick-out model for Zn in Si is confirmed by diffusion experiments under various conditions comprising both equilibrium and nonequilibrium of intrinsic point defects. From these experiments several properties of I and V including the enthalpies of formation and migration as the most important ones are determined. The results are given in Sec. V and compared to previous experimental results as well as theoretical calculations.

II. DIFFUSION IN SILICON

A. Self-diffusion

Self-diffusion experiments are of fundamental significance for studying intrinsic point defects in solids. Self-diffusion experiments were carried out using, e.g., the tracer ^{31}Si (Refs. 8–11) with a half-life time of about 2.6 h. However, this short-lived radiotracer limits the self-diffusion studies to a rather narrow temperature range near the melting point. Other self-diffusion experiments utilizing the stable isotop ^{30}Si in conjunction with secondary ion mass spectroscopy[12,13] or nuclear methods[14–16] have been carried out to avoid this difficulty but they all have their own disadvantages as, e.g.,

 ©1995 The American Physical Society

discussed by Frank *et al.*[17] Since both I and V may contribute to Si self-diffusion and also a direct exchange of adjacent Si atoms cannot be excluded,[18] $D_{\rm Si}^T$ can be written as

$$D_{\rm Si}^T = f_I C_I^{\rm eq} D_I + f_V C_V^{\rm eq} D_V + D_{\rm exchange}\,. \quad (2.1)$$

The first two terms represent a contribution of the interstitialcy and the vacancy mechanism to Si self-diffusion, respectively, where $C_{I,V}^{\rm eq}$ and $D_{I,V}$ are the equilibrium concentrations and the diffusion coefficients of I and V. $f_{I,V}$ are the correlation factors for the corresponding diffusion mechanism. They take into account that after a successful jump of a tracer atom the intrinsic point defect involved is next to the tracer which makes a reverse jump more probable. These correlation factors have been calculated by Compaan and Haven to f_V=0.5 (Ref. 19) and $f_I \approx 0.73$.[20] A direct exchange of adjacent Si atoms is additionally taken into account [last term in Eq. (2.1)] since total energy calculations by Pandey *et al.*[18] yield an activation energy of 4.3 eV for this mechanism, which agrees with experimentally determined values in the range of 4-5 eV for Si self-diffusion.[17]

As a main drawback, self-diffusion studies cannot determine the relative contribution of each individual self-diffusion mechanism. Further, self-diffusion is commonly considered to take place under thermal equilibrium conditions, i.e., the concentrations of I and V at the beginning of self-diffusion are equal to their thermal equilibrium values and these concentrations are not influenced by the self-diffusion process itself. Moreover, self-diffusion studies only yield information about the product of equilibrium concentration and diffusivity of the involved intrinsic point defect. This reflects the circumstance that a displacive jump of a Si lattice atom depends not only on its exchange frequency with I and V but also on the probability that such diffusion vehicle resides on an adjacent site. To complete the remarks concerning self-diffusion, we comment on the influence of electric charge carried by I and V. Vacancies in different charge states were identified by electron spin resonance (ESR) on electron irradiated Si samples while the associated electronic transition energies resulted from deep level transient spectroscopy (DLTS).[21,22] According to these studies a vacancy introduces two acceptor levels and two donor levels, the latter with negative-U property.[23] Different charge states are also assumed for the Si self-interstitial but not as generally accepted as are those for vacancies.[7] For diffusion temperatures yielding a much higher intrinsic carrier concentration than the free carrier concentration due to shallow dopants, the Fermi level lies in the middle of the band gap. Under these intrinsic conditions, the various charge states have fixed relative abundancies which hardly change with temperature. This justifies our approach to consider in the following only one self-diffusion term for I and V representing an average charge state.

B. Foreign-atom diffusion

In principle, information about intrinsic point defects can also be obtained by studying foreign-atom diffusion in Si. This, however, requires that I and/or V are involved in the diffusion process. Mainly interstitially dissolved foreign atoms (X_i) like, e.g., oxygen[24] or the 3d transition metals[25] are not suitable for revealing I or V properties since the direct interstitial diffusion of these elements does not involve intrinsic point defects. In contrast, mainly substitutionally dissolved foreign atoms (X_s) like the group III and V elements need vacancies or self-interstitials for diffusion as shown by surface oxidation or nitridation processes affecting both the dopant diffusion and stacking fault growth.[7,17] Ignoring the direct exchange mechanism, modeling of the diffusion behavior of mainly substitutionally dissolved foreign atoms X_s in Si is based on different point-defect reactions, summarized as

$$XI \rightleftharpoons X_s + I\,, \quad (2.2)$$

$$XV \rightleftharpoons X_s + V\,, \quad (2.3)$$

$$X_i \rightleftharpoons X_s + I\,, \quad (2.4)$$

$$X_i + V \rightleftharpoons X_s\,. \quad (2.5)$$

The first and second reaction are called the interstitialcy and vacancy mechanism, respectively. The defect pairs XI and XV suggest a coupling between foreign atom and intrinsic defects, e.g., due to Coulomb attraction and/or minimizing lattice distortion. The third and fourth reaction are known as the kick-out and the dissociative (or Frank-Turnbull) mechanism, respectively. They describe the diffusion behavior of hybrid elements which are dissolved on substitutional (X_s) as well as on interstitial (X_i) sites.

Focusing on the above reactions, a necessary condition to yield information about I and V is that these species control the reaction rate. In general, this situation occurs when the intrinsic point defect concentration deviates from its equilibrium value. Such nonequilibrium conditions can be created experimentally[7] by, e.g., electron radiation, implantation, oxidation, or nitridation of Si samples. In the case of surface oxidation, self-interstitials are injected whereas nitridation introduces vacancies into the Si lattice.[7] However, investigation of dopant diffusion under point defect injection conditions has provided a wealth of data about the dopant diffusion mechanism but not so much about the vacancies or self-interstitials involved.

Also the diffusion process of foreign atoms by itself can be responsible for nonequilibrium concentrations of intrinsic defects. This requires the relationship

$$C_{X_s}^{\rm eq} \gg C_V^{\rm eq}, C_I^{\rm eq} \quad (2.6)$$

to be fullfilled. In case of dislocation-free Si without effective internal sinks and/or sources for I and V, incorporation of X_s up to its solubility limit ($C_{X_s}^{\rm eq}$) consumes or produces according to the reactions (2.2) to (2.5) more V or I than the concentration existing in thermal equilibrium ($C_V^{\rm eq}$, $C_I^{\rm eq}$). Additionally, the supply of the dominating mobile foreign-atom species (XI, XV, or X_i) characterized by their transport capacities $C_{XI}^{\rm eq} D_{XI}$,

$C^{eq}_{XV}D_{XV}$, or $C^{eq}_{X_i}D_{X_i}$ must exceed the corresponding I- and V-related terms, i.e.,

$$C^{eq}_{XI}D_{XI}, C^{eq}_{XV}D_{XV}, C^{eq}_{X_i}D_{X_i} \gg C^{eq}_{V}D_{V}, C^{eq}_{I}D_{I}\,, \quad (2.7)$$

otherwise nonequilibrium concentrations of I and V locally induced by X_s incorporation decay more rapidly (by diffusion to the surface) than they are built up by foreign-atom supply (from the surface).

Foreign atoms in Si like Au,[26] Pt,[27] and Zn (Ref. 28) fulfill the conditions (2.6) and (2.7) ($C^{eq}_{X_i}D_{X_i} \gg C^{eq}_{V}D_{V}$, $C^{eq}_{I}D_{I}$). The diffusion of these elements into dislocation-free Si generates nonequilibrium of intrinsic point defects. Correspondingly, their diffusion behavior is characterized as I and/or V controlled. In the following, diffusion profiles of Zn in Si are presented whose properties are particularly suitable to get information about the intrinsic point defects. These results are shown to be more reliable than recent estimations based on Au and Pt profiles.

III. ZINC IN SILICON

A. Diffusion experiment

For Zn-diffusion experiments single-crystalline, dislocation-free floating-zone (FZ) Si wafers [(111) oriented, resistivity $\rho=10^4$ Ω cm, etch-pit density EPD=0] and plastically deformed FZ-Si bars with [12$\bar{3}$]-longitudinal axis and (111) and ($\bar{5}$41) lateral surfaces ($\rho=4\times10^3$ Ω cm, EPD=10^7–10^9 cm^{-2}) were cut into specimens of dimensions $9\times5\times(0.4$–$2)$ mm^3. The large surfaces were oriented along [111] direction. After mechanical and chemical polishing, samples were cleaned using the RCA procedure[29] to reduce organic as well as transition metal residues on the surfaces. After all treatments the samples were rinsed in deionized water.

The vapor pressure of Zn is high (boiling point at 907 °C) at temperatures commonly used for diffusion experiments. Therefore Zn diffusion in Si was carried out in closed quartz ampoules. In several experiments alternatively to elemental Zn (99.999%) a solution of Zn in HCl was used as diffusion source. The ampoule contained a quartz holder which carried the Si samples. In case of the elemental Zn source, an amount of about 30 mg was encapsulated by a thin quartz bulb inside the outer ampoule. In this way thermal equilibrium of the Si samples could be established by preannealing at the diffusion temperature without being exposed to Zn. After the preanneal phase, the ampoule mounted in a vertical resistance furnace was shaked, whereby the quartz bulb was destroyed by the quartz holder. This marked the start of the Zn-diffusion process which was terminated by plunging the ampoule into ethylene glycol at room temperature. In order to prevent condensation of Zn on the Si surfaces during cooling, a small amount of Si ($\approx$ 1 mg) was additionally given into the quartz bulb. As a further advantage this extra Si reduced the vapor pressure of Zn. This avoided breaking of the quartz bulb due to Zn-vapor pressure as high, as, e.g., 12 atm at about 1200 °C.[30] The main advantage of this Zn-diffusion method is the possibility to carry out isothermal diffusion anneals as short as a few seconds without substantial delay by heating up and cooling down.[31] This enabled us to follow in detail the Zn diffusion process also at early diffusion stages. The temperature was monitored with an accuracy of ±2 K by a calibrated Pt/PtRh thermocouple protected by an alumina tube contacting the ampoule.

Diffusion profiles of Zn were measured with the help of the spreading-resistance (SR) analysis. The calculation of concentration profiles needs the energy levels of Zn in the Si band gap affecting the electrical properties. First the electrical characterization of Zn in Si is treated before the concentration profiles obtained after Zn diffusion at different temperatures are presented.

B. Electrical characterization

Substitutional incorporated zinc (Zn_s) in Si is known to be a double acceptor.[32] The first acceptor stage ($Zn_s^{0/-}$) lies about 320 meV above the valence-band edge E_V as revealed by infrared absorption spectroscopy (319 ± 3 meV),[33,34] Hall effect measurements (325 ± 10 meV),[35] and DLTS (317 ± 9 meV) studies.[36] However, different ionization levels are reported for the second acceptor stage ($Zn_s^{-/2-}$). Carlson[37] observed a level at E_V+550 meV by Hall effect measurements whereas space charge capacitance techniques applied by Herman and Sah[32] yield a level at 617 meV above E_V. Furthermore Stolz *et al.*[36] reported a value of E_V+698 meV obtained by DLTS studies. Other levels related to Zn_s were also detected by DLTS (Refs. 32, 36, 38, and 39) and attributed to Zn_sB (Refs. 32 and 39) as well as Zn_s-donor pairs.[38] Identification of Zn-related defects was achieved by EPR investigations giving evidence for, e.g., monoclinic ZnCu and trigonal ZnCr pairs.[40] Several Zn-related levels are also known to be strongly influenced by the thermal history.[36,39] Therefore, we have to check whether our diffusion procedure may lead to the formation of unwanted complexes between, e.g., Zn and transition metal contaminants like Fe, Cu, or Ni. This is especially important as we utilize SR analysis to determine Zn penetration profiles. To gain a solid base for calculating concentration profiles from SR measurements, we checked by DLTS the energy levels originating from Zn diffusion (and additional annealing). For this purpose dislocation-free and highly dislocated boron-doped samples with specific resistivities of 1.9 Ω cm and 1.7 Ω cm were diffused with Zn at 1115 °C and 1021 °C for 200 s and 20 min, respectively, and rapidly quenched to room temperature. Schottky diodes were prepared by evaporation of aluminum whereby care was taken to avoid an additional thermal exposure. DLTS spectra of Zn-diffused dislocation-free Si samples being either only quenched to room temperature or additionally heat-treated at 600 °C are illustrated in Fig. 1 as solid and dashed lines, respectively. The maxima at T=167 K and T=301 K corresponding to the energy levels $E_V+0.28$ eV and $E_V+0.58$ eV are attributed to the Zn_s double acceptor states $Zn_s^{0/-}$ and $Zn_s^{-/2-}$, respectively. These lev-

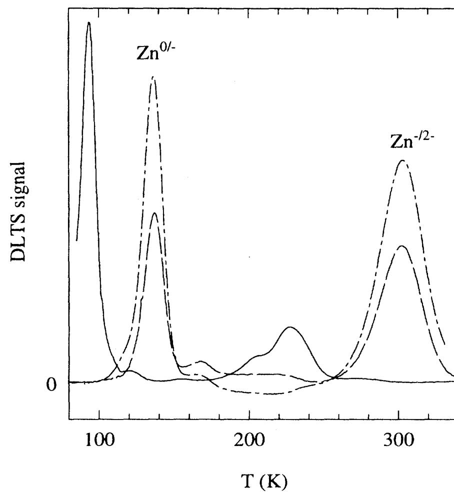

FIG. 1. DLTS spectra of a dislocation-free (solid line) and highly dislocated (dash-dotted line) B-doped Si sample which was diffused with Zn at 1115 °C (200 s) and 1021 °C (20 min), respectively, and rapidly quenched to room temperature. Dashed line, DLTS spectra of the dislocation-free Si sample after an additional heat treatment at 600 °C for 15 min.

els appear always after the additional 600 °C treatment, whereas the maximum at T=93.5 K corresponding to a level at E_V+0.17 eV dominates directly after quenching. In contrast, the energy states of the Zn double acceptor dominate in highly dislocated Si even immediately after quenching as verified through Fig. 1 (see dash-dotted line). The thermal activation of the Zn_s double acceptor states in dislocation-free Si confirms recent DLTS results from Zn-doped samples obtained by Weiss *et al.*[39] and Stolz *et al.*[36] The discrepancies to the energy levels determined by infrared absorption spectroscopy are not serious since ionization energies extracted from DLTS spectra were usually evaluated assuming temperature-independent capture cross sections. Stolz *et al.*[36] reported that the energy positions of the Zn_s levels strongly depend on the electric field applied. Taking into account this Poole-Frenkel effect the energy level of $Zn_s^{0/-}$ was corrected from initial 252 meV to 317 meV above E_V achieving a good agreement with the results obtained by infrared absorption spectroscopy.[33,34]

C. Spreading-resistance analysis

The thermal sensitivity of Zn-related levels especially in dislocation-free Si is also supported by SR profiles recorded on perpendicular inner cross sections of Zn-diffused samples. As an example Fig. 2(a) shows SR profiles from dislocation-free samples either immediately measured after Zn diffusion at 1115 °C for 240 s stopped by rapid quenching to room temperature or after an additional heat treatment at 600 °C of about 900 s. This plot with penetration depth normalized to the sample thickness d illustrates symmetrical in-diffusion of Zn from two opposite surfaces. As is seen, the SR profile obtained after additional annealing deviates considerably from the profile associated with the quenched sample. In contrast, the SR profiles of a simultaneously Zn-diffused highly dislocated Si sample are not affected by the additional heat treatment. This is shown in Fig. 2(b). In accord with the results obtained by DLTS the Zn_s double acceptor dominates in highly dislocated Si even immediately after quenching.

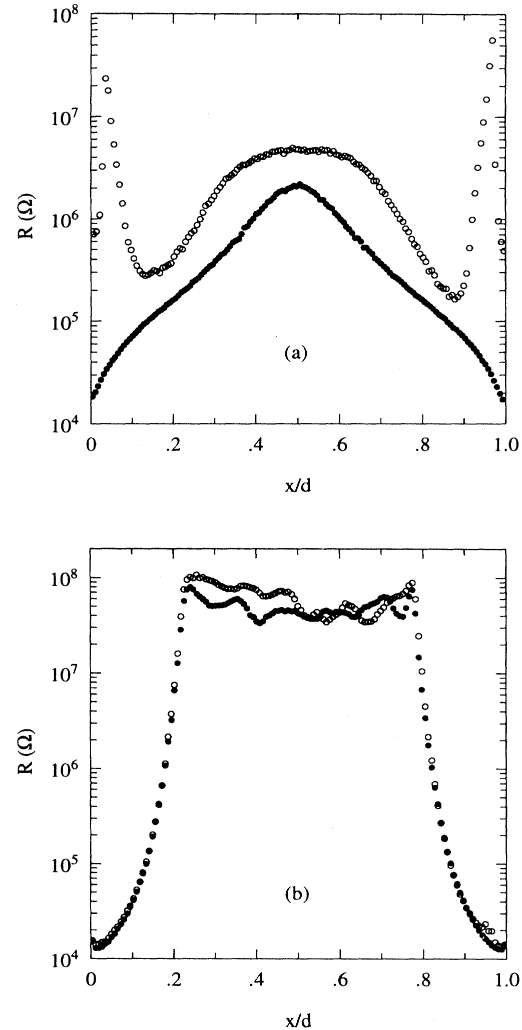

FIG. 2. Spreading-resistance profiles measured after Zn diffusion at 1115 °C (240 s) in (a) dislocation-free Si (d=1435 μm) and (b) highly dislocated Si (d=1310 μm) before (○) and after (•) an additional heat treatment at 600 °C of about 900 s. The penetration depth is normalized by the sample thickness d.

In summary, our analysis shows that the treatment at 600 °C activates the Zn_s double acceptor states in Zn-diffused dislocation-free Si. This treatment is indispensable for the present aim of following the diffusion-induced incorporation of Zn_s with the aid of spreading-resistance analysis. We claim that the depth distribution of Zn_s does not change by the 600 °C anneal. This is evidenced

by the SR profiles in highly dislocated Si which are equal before and after the additional annealing [see Fig. 2(b)]. Regarding dislocation-free Si we have strong indications that during cooling from the diffusion temperature Zn_s forms pairs or complexes with unwanted transition metal atoms like, e.g., Cu which greatly affects the energy level scheme. Very probably, 600 °C annealing releases these unwanted elements from Zn_s. In highly dislocated Si they are very likely trapped by the dislocations so that Zn_s remains isolated during fast quenching from the diffusion temperature.

Spreading-resistance analysis of the high-Ohmic Si starting material annealed at the diffusion temperature for several hours but without being exposed to Zn yields a homogeneous resistance of about 10^8 Ω. This shows that contamination by electrically active impurities may be neglected. Therefore spreading resistances of 10^7 Ω and below measured after Zn diffusion are caused by incorporation of Zn. Profiles measured on the same Zn-diffused sample mutually agree even for $R \gtrsim 10^7$ Ω.

Since resistivities obtained by a two point probe measurement (Solid State Measurements, ASR-100B) depend on the radius of the contact area of the probes as well as on the barrier resistance between the probes and the Si surface,[41] homogeneously boron-doped Si samples with well-known resistivities ρ are used for calibration. 12 calibration samples with ρ between 1 Ω cm and 20 000 Ω cm yield spreading resistances R in the range of 10^3–10^8 Ω, significant for the present Zn-diffused samples. With the help of so-obtained calibration curves, SR profiles were converted into resistivity profiles. Then Zn_s concentration profiles can be calculated taking into account the Zn_s double acceptor states of 320 meV and 620 meV above E_V obtained by infrared absorption spectroscopy.[33,34] This procedure has already been described by Grünebaum *et al.*[28] Notably, the concentration is mainly given by the well-confirmed level of the first ionization stage. The deep level associated with the second ionization stage does not crucially enter the calculation of concentrations so that its lower reliability is not relevant. Typically, spreading resistances of 10^4 Ω and 10^7 Ω correspond to Zn_s concentrations of about 5×10^{16} cm^{-3} and 10^{13} cm^{-3}, respectively. To record Zn_s distributions as good as possible calibration was carried out about every 1000 steps of the SR probe. This effort precluded any probe-tip wear effects on the measurements. Moreover, it was checked repeatedly that changes in probe-tip condition after many steps do not influence the *shape* of Zn_s profiles but at most absolute concentration. Therefore, the Zn_s profiles reported here are normalized to the corresponding boundary concentration. For absolute reference we rely on neutron activation data previously published.[28]

D. Results

1. Characteristic zinc profiles

Figure 3 shows Zn_s concentration profiles $C_{Zn_s}(x)$ resulting from SR measurements on dislocation-free Si [profile (a)] and a highly dislocated sample [profile (c)] which were simultaneously Zn-diffused at 1115 °C for 2880 s and additionally heat treated at 600 °C. The boundary concentration is about $C_{Zn_s}(x{=}0){=}2.5\times10^{16}$ cm^{-3} at this temperature and corresponds for the used pure Zn-diffusion source to the pertaining Zn solubility. This value complies within the accuracy of SR with the solubility limit of Zn in Si at 1115 °C as determined by neutron activation analysis of homogeneously Zn-doped samples.[28] Also shown in Fig. 3 is a Zn_s concentration profile in dislocation-free Si obtained after 1620 s of Zn diffusion at 1115 °C using a 0.1 molar solution of Zn in HCl as diffusion source [profile (b)]. This source yields $C_{Zn_s}(x=0){=}4.5\times10^{14}$ cm^{-3} which is a factor 55 smaller than the solubility limit at 1115 °C attained in equilibrium with the elemental vapor source. Inspecting the shape of the profiles in Fig. 3 reveals that the profile in dislocation-free Si is convex whereas the profile in the simultanously diffused highly dislocated Si is concave. Also the lower profile (c) has a concave curvature. Obviously, in dislocation-free Si the profile shape changes from convex to concave when the thermodynamic activity of the Zn source is lowered. A similar change occurs when under identical conditions the dislocation density increases from zero to, e.g., 10^8 cm^{-2}. This shows diffusion of Zn in Si to be very sensitive on the defect structure of the substrate as well as on the prevailing ambient conditions. In preview of the theoretical description of these profiles treated in Sec. IV, the above experimental observations constitute crucial evidence that Zn in Si mainly diffuses via the kick-out mechanism. Only this mechanism yields a consistent description of all profiles in Fig. 3 as illustrated by the solid lines.

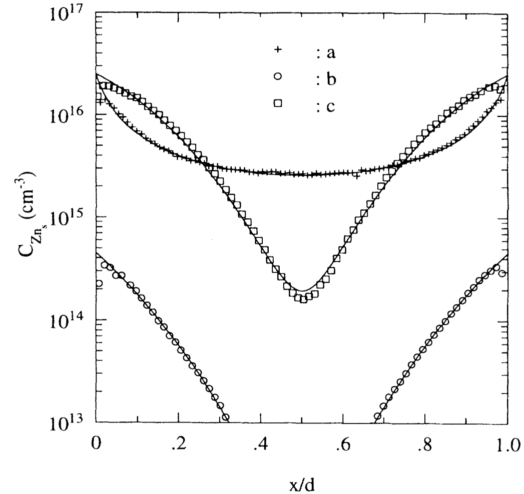

FIG. 3. Concentration profiles of substitutional Zn resulting from SR measurements performed on dislocation-free (profile *a*) and highly dislocated (profile *c*) Si samples Zn diffused at 1115 °C for 2880 s using elemental Zn as a diffusion source. Profile *b*, Zn_s profile in dislocation-free Si due to Zn diffusion at 1115 °C for 1620 s using a solution of Zn in HCl as a diffusion source. Solid lines, theoretical kick-out profiles simultaneously fitted to the data by optimizing the two essential parameters $C^{eq}_{Zn_i}D_{Zn_i}$ and $C^{eq}_I D_I$.

2. *Time evolution at different temperatures*

The time evolutions of Zn_s incorporation resulting from SR measurements on dislocation-free Si which was Zn-diffused at temperatures between 1208 and 870 °C applying our short-time diffusion method are displayed in Figs. 4 and 5, respectively. The preanneal was chosen to 1 h at 1208 °C up to 4 h at 870 °C. Time periods chosen for diffusion and thicknesses d of the Si samples are listed in Table I. Concentrations of substitutional dissolved Zn are normalized by the boundary concentration $C_{Zn_s}(x = 0)$. This concentration could be obtained more accurately by SR analysis on highly dislocated Si samples diffused simultaneously at this temperature[42] than on dislocation-free Si, regarding the profile shape in the near surface regime. Typical examples for Zn_s profiles in highly dislocated Si after diffusion at 1021 °C for different diffusion times are shown in Fig. 4(d). The time evolutions of Zn_s concentration profiles in highly dislocated Si measured at other temperatures than 1021 °C are presented in Refs. 42 and 43. The solid lines in Figs. 4 and 5 already show the result of successful fitting of all experimental profiles which is mainly based on the kick-out model [Figs. 4(a)–4(c), Figs. 5(a) and 5(b)] and to a minor extent also on the dissociative diffusion mechanism [Figs. 5(c) and 5(d)]. The solid lines in Fig. 4(d) represent the best fits achieved with complementary error functions. The numerical analysis of Zn-diffusion profiles is discussed in Sec. IV C in detail. In the next section the basic equations for a mathematical treatment of foreign-

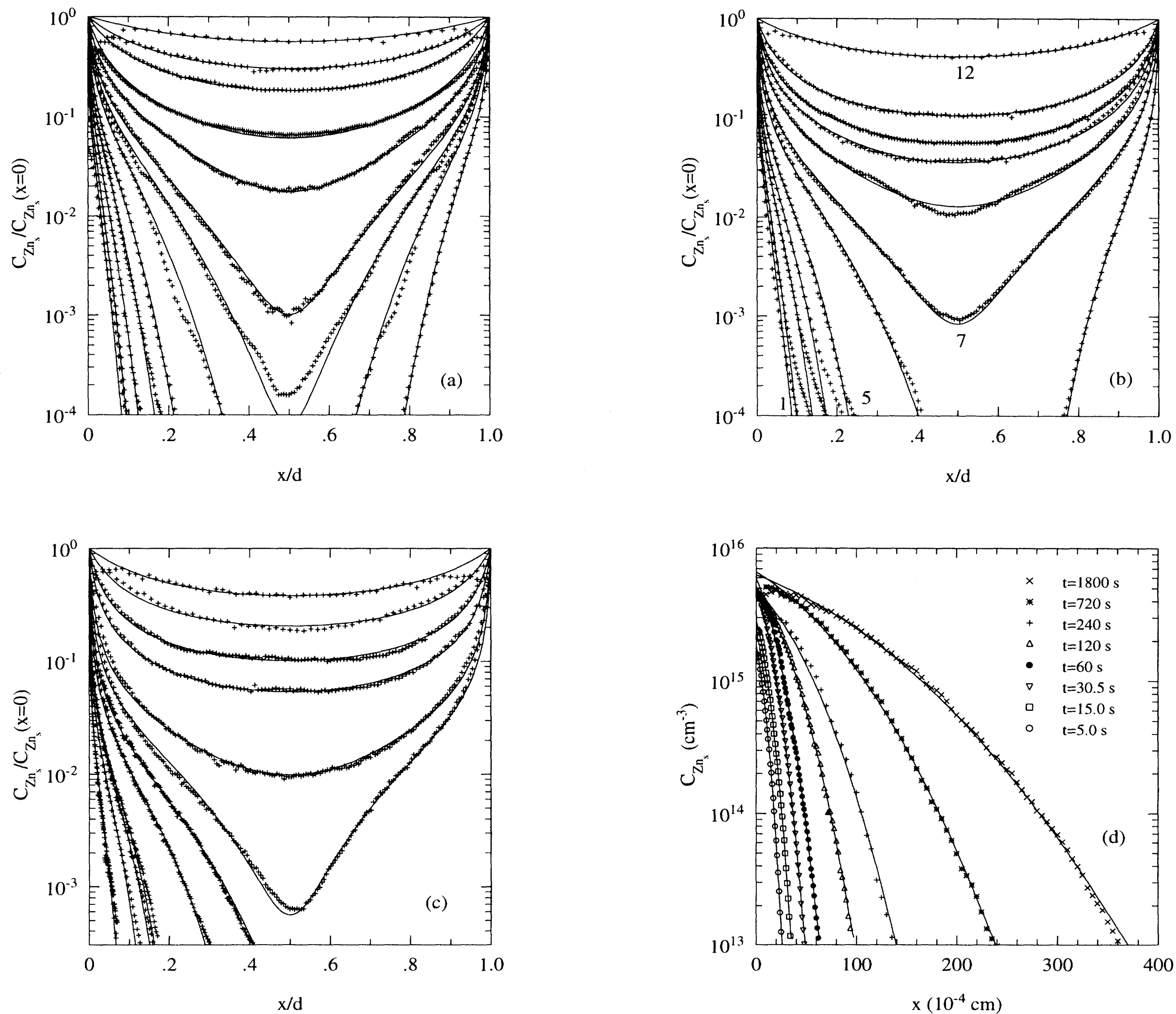

FIG. 4. *Dislocation-free Si* (a)–(c): Zn_s-concentration profiles measured by SR after Zn diffusion at (a) 1208 °C, (b) 1115 °C, and (c) 1021 °C for diffusion times listed in Table I. Solid lines show calculated profiles based on the kick-out model applying one set of parameters for each temperature. Numbers in diagram (b) indicate order with respect to diffusion time (cf. Table I). *Highly dislocated Si* (d), Zn_s concentration profiles after diffusion at 1021 °C for different diffusion times. Solid lines show successful fitting by complementary error functions.

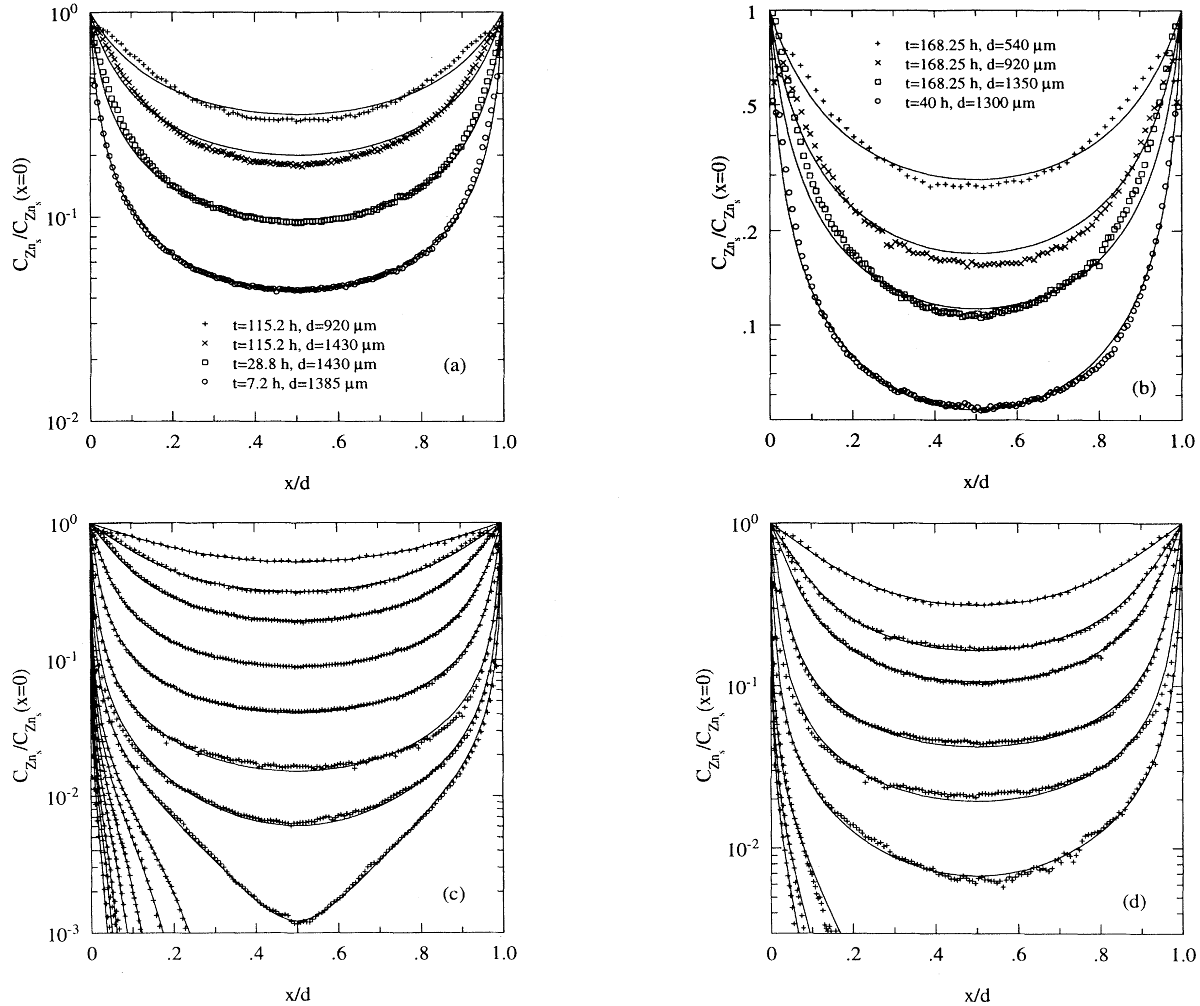

FIG. 5. Zn_s concentration profiles after diffusion into dislocation-free Si at (a),(c) 942 °C and (b),(d) 870 °C for time periods listed in Table I. Calculated profiles (solid lines) are based on the kick-out mechanism alone (a),(b) or on the kick-out and dissociative mechanism simultaneously (c),(d) applying one set of parameters for each temperature.

TABLE I. Diffusion times t and sample thicknesses d of Si samples Zn diffused at temperatures between 870 and 1208 °C.

870 °C		942 °C		1021 °C		1115 °C		1208 °C	
t (s)	d (μm)	t (s)	d (μm)	t (s)	d (μm)	t (s)	d (μm)	t (s)	d (μm)
120	1350	5.0	1400	5.0	1430	2.8	1310	2.5	1540
240	1340	10.0	1400	15.0	1335	5.0	1430	5.0	1780
720	1305	15.0	1410	30.5	1420	10.0	1340	7.5	1580
8640	1350	30.0	1410	60.0	1820	19.5	1420	15.0	1590
34560	1305	60.0	1400	120	1440	60.0	1800	30.0	1680
144000	1300	120	1400	240	1440	120	1445	64.0	1535
605700	1350	240	1450	720	1780[a]	240	1435	120	1520
605700	920	720	1340	1800	1670	720	1400	240	1690
605700	540	2160	1400	5400	1140	720	910	720	1710
		6480	1420	16200	1230	2880	1415	2160	1850
		25920	1385	16200	580	2880	915	2160	950
		103680	1430	16200	300	11520	545	2160	630
		414720	1430					2160	340
		414720	920						
		414720	580						

[a]After preferential etching this Si sample shows a small defect density which probably arises from I precipitation. Therefore, a defect density $\rho_d \approx 8\times10^2$ cm^{-2} was taken into account for fitting the corresponding experimental Zn_s profile.

atom diffusion governed by the kick-out mechanism are given. Based on these equations, theoretical predictions are derived leading to a deep insight into the observed Zn-diffusion behavior.

IV. KICK-OUT DIFFUSION MECHANISM

A. Theoretical predictions

1. Basic equations

The kick-out mechanism (2.4) is one of the so-called interstitial-substitutional diffusion mechanisms which mediates the transformation of an isolated interstitial foreign atom X_i to a substitutional foreign atom X_s thereby creating a Si self-interstitial I. This reaction was first proposed for the diffusion of gold in Si.[26] Regarding the foreign atoms Au, Pt, and Zn it can be stated that the solubilities $C_{X_i}^{\rm eq}$ and $C_{X_s}^{\rm eq}$ are always much lower than the Si atom density $C_{\rm O}(=5.0\times10^{22}\ {\rm cm}^{-3})$. As a consequence the number of Si atoms on lattice sites remains practically constant during the diffusion-reaction process whereas the concentrations of X_i, X_s, and I may change strongly. Furthermore, we consider that the foreign-atom diffusion takes places under electronically intrinsic conditions. This is fullfilled for Zn, Au, and Pt in Si even at their maximum solubility of about 10^{17} cm^{-3} attained at 1300 °C.[28,44,45] Foreign-atom transport via the direct exchange or the vacancy mechanism is certainly small compared to that via foreign-atom interstitials, i.e., $D_{X_s}\approx 0$. Under the above conditions diffusion by the kick-out mechanism is described by the following partial differential equations (PDE's):[31]

$$\frac{\partial \widetilde{C}_{X_s}}{\partial t} = k_{-2}C_I^{\rm eq}\left(\widetilde{C}_{X_i} - \widetilde{C}_{X_s}\widetilde{C}_I\right) , \tag{4.1}$$

$$\frac{C_{X_i}^{\rm eq}}{C_{X_s}^{\rm eq}}\frac{\partial \widetilde{C}_{X_i}}{\partial t} = D_{X_i}^{*}\frac{\partial^2 \widetilde{C}_{X_i}}{\partial x^2} - \frac{\partial \widetilde{C}_{X_s}}{\partial t}, \tag{4.2}$$

$$\frac{C_I^{\rm eq}}{C_{X_s}^{\rm eq}}\frac{\partial \widetilde{C}_I}{\partial t} = D_I^{*}\frac{\partial^2 \widetilde{C}_I}{\partial x^2} + \frac{\partial \widetilde{C}_{X_s}}{\partial t} + k_I^{*}(1-\widetilde{C}_I) . \tag{4.3}$$

The equilibrium constant K of reaction (2.4) is given by

$$K = \frac{k_{+2}}{k_{-2}} = \frac{C_{X_s}^{\rm eq}C_I^{\rm eq}}{C_{X_i}^{\rm eq}C_{\rm O}} \tag{4.4}$$

applying the mass law of action. This interrelation between the reaction rate constants for forward k_{+2} and backward k_{-2} reaction was taken into account in the derivation of Eqs. (4.1)–(4.3). The above PDE's hold for one-dimensional geometry characterized by penetration depth x, diffusion time t, concentrations $\widetilde{C}_m = C_m(x,t)/C_m^{eq}$ normalized to their equilibrium values $C_m^{\rm eq}$ $(m\in\{X_s,X_i,I\})$, and the reduced diffusivities $D_n^{*} = C_n^{\rm eq}D_n/C_{X_s}^{\rm eq}$ $(n\in\{X_i,I\})$. The last term in Eq. (4.3) accounts for annihilation of I at internal sinks like, e.g., dislocations. The efficiency of this process was estimated to $k_I^{*}\approx\rho_d D_I^{*}$,[26] reflecting the diffusion-limited case with dislocation density ρ_d. The above PDE's contain five temperature-dependent parameters $D_{X_i}^{*}$, D_I^{*}, $C_{X_i}^{\rm eq}/C_{X_s}^{\rm eq}$, $C_I^{\rm eq}/C_{X_s}^{\rm eq}$, and $k_{-2}C_I^{\rm eq}$, which determine the interstitial-substitutional diffusion process at all diffusion times under given boundary and initial conditions.

After sufficient long diffusion times local equilibrium of the kick-out reaction is reached which is characterized by

$$\widetilde{C}_{X_s}\widetilde{C}_I = \widetilde{C}_{X_i} . \tag{4.5}$$

For these conditions it will be shown below that the PDE's reduce to

$$\frac{\partial \widetilde{C}_{X_s}}{\partial t} = \frac{\partial}{\partial x}D_{\rm eff}\frac{\partial \widetilde{C}_{X_s}}{\partial x} . \tag{4.6}$$

Taking into account Eq. (2.6) necessary for I-controlled diffusion and

$$C_{X_s}^{\rm eq} \gg C_{X_i}^{\rm eq} , \tag{4.7}$$

which is fulfilled for mainly substitutional dissolved foreign atoms like Au, Pt, and Zn in Si, the effective diffusion coefficient $D_{\rm eff}$ in Eq. (4.6) is given for different experimental conditions in the following.

2. Dislocation-free Si

High boundary concentrations. In dislocation-free Si ($\rho_d=0$) no sinks for self-interstitials exist. The high boundary concentration maintains

$$C_{X_i}^{\rm eq}D_{X_i} \gg C_I^{\rm eq}D_I \tag{4.8}$$

representing Eq. (2.7) in case of diffusion via the kick-out mechanism only. Then the supply of X_i from the surface occurs more rapidly than the decay of the I supersaturation by outdiffusion toward the surface. At long diffusion times $\widetilde{C}_{X_i}\approx 1$ already holds whereas the distribution of I still deviates from the equilibrium state. In this diffusion regime and additionally taking into account Eq. (4.5), Eq. (2.6), and Eq. (4.7), the PDE's (4.1)–(4.3) reduce to Eq. (4.6) with the concentration-dependent diffusion coefficient[26]

$$D_{\rm eff}^{(a)} = \frac{C_I^{\rm eq}D_I}{C_{X_s}^{\rm eq}}\left(\frac{C_{X_s}^{\rm eq}}{C_{X_s}}\right)^2 = \frac{D_I^{*}}{\widetilde{C}_{X_s}^2} . \tag{4.9}$$

$D_I C_I^{\rm eq}(=D_I^{*}C_{X_s}^{\rm eq})$ denotes the self-interstitial contribution to the uncorrelated Si self-diffusion coefficient. Based on Eq. (4.6), a convenient expression for $\widetilde{C}_{X_s}$ in the center of the Si sample with thickness d can be deduced:[26]

$$\widetilde{C}_{X_s}\left(\frac{d}{2},t\right) = \left(4\pi D_I^{*}\frac{t}{d^2}\right)^{\frac{1}{2}} . \tag{4.10}$$

This equation holds for sufficient long diffusion times but

fails of course for times longer than those necessary to saturate the sample. In this long-time regime Zn_s profiles in semilogarithmic representation are distinctly U-shaped like profile (a) in Fig. 3, while the associated I distribution has an inverse appearance because of $\widetilde{C}_I \approx 1/\widetilde{C}_{Zn_s}$ [see Eq. (4.5) and $\widetilde{C}_{X_i} \approx 1$]. These features reflect that Zn_s incorporation is hampered by outdiffusion of I toward the sample surface.

Low boundary concentration. During Zn diffusion the Dirichlet-boundary condition $C_{X_i}(0,t) = C^{\rm eq}_{X_i}$ is achieved by a constant Zn vapor pressure in the diffusion ampoule. This vapor pressure also determines the Zn_s equilibrium concentration $C^{\rm eq}_{X_s}$ which is proportional to $C^{\rm eq}_{X_i}$ whereas the properties D_{X_i}, $C^{\rm eq}_I$, and D_I are not influenced by the ambient conditions. Also the equilibrium constant K [see Eq. (4.4)] of reaction (2.4) depends on temperature only. Combining all these dependencies, the parameters $C^{\rm eq}_{X_i}/C^{\rm eq}_{X_s}$, $D^*_{X_i}$, and $k_{-2}C^{\rm eq}_I$ remain unchanged upon, e.g., decreasing the vapor pressure whereas D^*_I and $C^{\rm eq}_I/C^{\rm eq}_{X_s}$ will increase. Therefore, at sufficiently low boundary concentrations the relationship

$$C^{\rm eq}_{X_i} D_{X_i} \ll C^{\rm eq}_I D_I \tag{4.11}$$

may be fullfilled. As a consequence X_i-X_s exchange cannot establish I supersaturation and $\widetilde{C}_I \approx 1$ holds during the whole diffusion process. Taking into account this condition and Eqs. (4.5), (2.6), and (4.7), the PDE's (4.1)–(4.3) reduce to Eq. (4.6) with the effective diffusion coefficient

$$D^{(b)}_{\rm eff} = \frac{C^{\rm eq}_{X_i} D_{X_i}}{C^{\rm eq}_{X_s} + C^{\rm eq}_{X_i}} \approx D^*_{X_i}\,. \tag{4.12}$$

In case of a constant surface concentration $C^{\rm eq}_{X_s}$ the solution of Eq. (4.6) is given by

$$\widetilde{C}_{X_s}(x,t) = {\rm erfc}\frac{x}{2\sqrt{D^*_{X_i} t}}\,. \tag{4.13}$$

Under these diffusion conditions Zn_s profiles are described by a complementary error function like profile (b) in Fig. 3.

3. *Highly dislocated Si*

In Si containing extended defects like, e.g., dislocations a supersaturation of self-interstitials can also decay by I annihilation at these defects. Assuming a diffusion limited annihilation process, the mean distance between dislocations is given by $x_d = 1/(\sqrt{\rho_d})$ yielding $x_d \approx 1$ μm for plastically deformed Si with $\rho_d \approx 10^8$ cm^{-2}. At penetration depths x for which

$$\frac{x^2}{D^*_{X_i}} > \frac{x_d^2}{D^*_I} \tag{4.14}$$

holds, the annihilation of self-interstitials at internal sinks occurs more rapidly ($t_d = x_d^2/D^*_I$) than the supply of X_i from the surface ($t = x^2/D^*_{X_i}$). Then at penetration depths fulfilling Eq. (4.14) no I supersaturation is created due to the X_i-X_s exchange. For Zn diffusion in Si between 1208 and 870 °C $D^*_{Zn_i}/D^*_I \gtrsim 100$ holds. This yields $x > 5$ μm as penetration depth where I mainly annihilates at internal sinks while in the regime $x \lesssim 5$ μm the surface acts as a major sink. Since all Zn_s profiles even for the shortest diffusion times exceed this penetration depth drastically [see, e.g., Fig. 4(d)], $\widetilde{C}_I(x,t) \approx 1$ holds regardless of the existing boundary concentration $C_{X_s}(x=0)$. As a consequence the above PDE system is reduced to Eq. (4.1) with $\widetilde{C}_I = 1$ and Eq. (4.2) containing the three parameters $D^*_{X_i}$, $C^{\rm eq}_{X_i}/C^{\rm eq}_{X_s}$, and $k_{-2}C^{\rm eq}_I$.[42] For local equilibrium and mainly substitutional dissolved foreign atoms expressed by Eqs. (4.5) and (4.7), respectively, the two PDE's can be further simplified to Eq. (4.6) with

$$D^{(c)}_{\rm eff} = D^*_{X_i}\,. \tag{4.15}$$

If the surface concentration is constant [$\widetilde{C}_{X_s}(x=0,t)=1$], Zn_s profiles in highly dislocated Si are described by a complementary error function [Eq. (4.13)] like profile (c) in Fig. 3.

B. Evidence for the kick-out mechanism of Zn in Si

1. *Zn_s profile shape*

The predictions of the kick-out model outlined above are observed for Zn in Si. This is illustrated by the profiles (a), (b), and (c) in Fig. 3. For long-time diffusion into dislocation-free Si with high boundary concentration Zn_s profiles [see profile (a)] are U-shaped in semi-logarithmic representation with the concentration-dependent effective diffusion coefficient $D^{(a)}_{\rm eff}$ [Eq. (4.9)]. Diffusion of Zn into dislocation-free Si under low concentration conditions leads according to Eq. (4.13) to erfc-type profiles due to a constant diffusivity $D^{(b)}_{\rm eff}$ [Eq. (4.12)]. Evidence is given by profile (b) in Fig. 3. To our knowledge this represents the first demonstration of boundary-concentration dependence of foreign-atom diffusion described by interstitial-substitutional diffusion mechanisms. Also in highly dislocated Si, Zn diffusion induces erfc-shaped profiles as shown by profile (c) in Fig. 3. Since this profile runs parallel to profile (b), one may conclude that $D^{(b)}_{\rm eff} \approx D^{(c)}_{\rm eff}$ in agreement with Eqs. (4.12) and (4.15).

The kick-out mechanism as diffusion model for Zn in Si is even more reliable as the solid lines in Fig. 3 are theoretical profiles calculated on the basis of one set of model parameters solving Eqs. (4.1)–(4.3) numerically. This was done using a software package provided by Jüngling *et al.*[46] Comparison of experimental and calculated $\widetilde{C}_{Zn_s}(x,t)$ was performed by PROFILE[47] in order to extract the parameters D^*_I and $D^*_{Zn_i}$ by error minimization. From the simultaneous fitting taking into account the effect of high and low boundary concentrations we obtain the parameters $D^*_I = 4.98 \times 10^{-9}$ cm^{-2} s^{-1} and

$D^*_{Zn_i}=1.14\times10^{-7}$ cm^{-2} s^{-1} which mainly determine profile (a) and the profiles (b) and (c) in Fig. 3, respectively.

2. Zn_s concentration at $x = d/2$

Concentrations of Zn_s in the center of dislocation-free Si samples are displayed in Fig. 6 for all measurements at five different temperatures. The time dependence of $\widetilde{C}_{Zn_s}(d/2)=C^m_{Zn_s}/[C_{Zn_s}(x=0)]$ according to Eq. (4.10) is shown in this double logarithmic plot as solid lines. Concentrations $\widetilde{C}_{Zn_s}(d/2)$ well described by Eqs. (4.10) belong to the long-time diffusion regime governed by the diffusion coefficient D^*_I. The good agreement between kick-out theory and Zn-diffusion experiment in this high concentration, long-time regime provides further evidence that the kick-out mechanism prevails for Zn in Si. Data of D^*_I resulting from the straight-line fits in Fig. 6 are listed in Table II. This table also contains D^*_I values extracted from the full set of Zn_s profiles at one temperature by solving Eqs. (4.1)–(4.3) numerically. These data deviate at higher temperatures from the results obtained analytically with the aid of the relationship (4.10). The numerical analysis treated in detail in Sec. IV C shows that particularly at high temperatures $\widetilde{C}_{Zn_i}(d/2)$ remains below unity even after the longest diffusion times. Consequently, in those cases extraction of D^*_I based on Eq. (4.10), which was derived under the assumption of $\widetilde{C}_{Zn_i}\approx1$, must fail.

From D^*_I and $C^{eq}_{Zn_s}$ at each temperature the self-interstitial component of the uncorrelated self-diffusion coefficient $C^{eq}_I D_I$ can be calculated since $C^{eq}_{Zn_s}D^*_I=C^{eq}_I D_I$. The present finding that the $C^{eq}_I D_I$ data so-obtained are very close to experimentally determined Si self-diffusivities also supports the kick-out model for Zn in Si.[28] A more detailed discussion of self-diffusion related data is postponed until Sec. IV C.

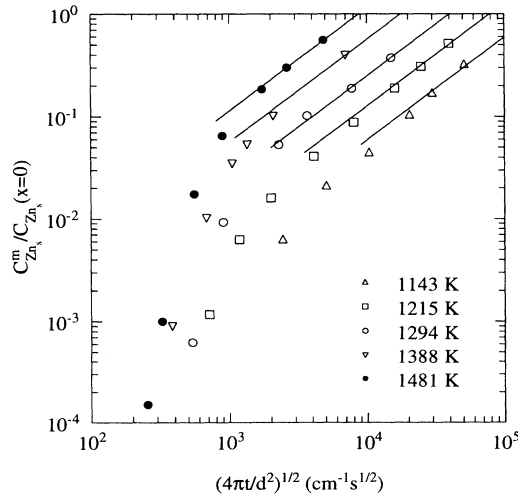

FIG. 6. Zn_s concentration in the center of a Si sample, $C^m_{Zn_s}/C_{Zn_s}(x=0)$, as a function of $(4\pi t/d^2)^{0.5}$ (t=annealing time, d=thickness of the sample).

TABLE II. Reduced diffusion coefficients $D^*_I=C^{eq}_I D_I/C^{eq}_{Zn_s}$ deduced by analytical and numerical analysis of Zn-diffusion profiles in dislocation-free Si.

	D^*_I (cm^2 s^{-1})	
T (°C)	analytical	numerical
870	3.5×10^{-11}	$(3.8\pm0.3)\times10^{-11}$
942	1.6×10^{-10}	$(1.8\pm0.1)\times10^{-10}$
1021	6.2×10^{-10}	$(7.8\pm0.3)\times10^{-10}$
1115	3.1×10^{-9}	$(5.0\pm0.1)\times10^{-9}$
1208	1.3×10^{-8}	$(2.3\pm0.1)\times10^{-8}$

3. Formation of I precipitates

Self-interstitial supersaturation due to Zn_s incorporation by the kick-out reaction in dislocation-free Si can decay not only by I diffusion to the sample surfaces but also by nucleation and growth of I precipitates. Apparently precipitation is favored when the highest supersaturation which arises in the center of the Si samples exceeds an upper limit. The so-initiated collapse of $\widetilde{C}_I$ leads to locally enhanced Zn_s incorporation because $\widetilde{C}_{Zn_s}\approx1/\widetilde{C}_I$. As a result the Zn_s profile evolves from the known U shape into a so-called W shape. Figure 7 displays such a W-shaped profile measured after 11 520 s of Zn diffusion at 1115 °C. Sirtl etching of an inner surface shows several stacking faults in the center of the Si sample. Very likely, these stacking faults are extrinsic in nature and thus constitute a special form of I precipitates. W-shaped profiles in conjunction with extrinsic stacking faults were also observed after diffusion of Au in Si.[48] This shows participation of Si self-interstitials in Zn (and Au) diffusion in Si consistent with the kick-out model.

C. Numerical analysis of zinc diffusion and results

1. Initial and boundary conditions

Under the particular conditions established by the present diffusion procedure (Sec. III A) the formulation

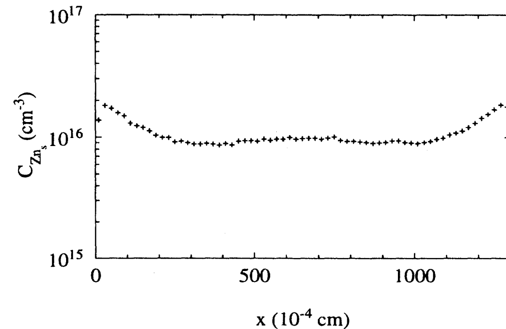

FIG. 7. Zn_s profile influenced by the formation and growth of stacking faults in the center of an initially dislocation-free Si sample after 11520 s of diffusion at 1115 °C.

of initial and boundary conditions for the numerical calculations is straightforward. Preannealing without Zn justifies to characterize the initial conditions by

$$\widetilde{C}_{\mathrm{Zn}_s}(x,0) = \widetilde{C}_{\mathrm{Zn}_i}(x,0) = 10^{-10} , \quad (4.16)$$

$$\widetilde{C}_I(x,0) = 1 . \quad (4.17)$$

The initial condition (4.16) complies with Zn_s concentrations in the sample far below the SR detection limit of 10^{12}–10^{13} cm^{-3}. The boundary conditions for $t \geq 0$ are given by

$$\widetilde{C}_{\mathrm{Zn}_s}(0,t) = \widetilde{C}_{\mathrm{Zn}_s}(d,t) = 1 - \exp(-k_{-2}C_I^{\mathrm{eq}}t) , \quad (4.18)$$

$$\widetilde{C}_{\mathrm{Zn}_i}(0,t) = \widetilde{C}_{\mathrm{Zn}_i}(d,t) = 1 , \quad (4.19)$$

$$\widetilde{C}_I(0,t) = \widetilde{C}_I(d,t) = 1 . \quad (4.20)$$

Equation (4.18) represents the solution of the PDE's (4.1)–(4.3) at $x = 0$. Due to Eq. (4.18), the increase of Zn_s at the surface directly depends on the rate constant k_{-2}. Up to now interstitial-substitutional reaction rates were unimportant for the analysis of diffusion experiments. In conventional diffusion experiments the X_i-X_s exchange is very fast as compared to the diffusion times involved. Fortunately, our procedure for short-time Zn diffusion enabled us to measure such rate constants from the increase of the Zn_s boundary concentration.

2. Diffusion into highly dislocated Si

Figure 4(d) shows Zn_s profiles after Zn diffusion at 1021 °C in highly dislocated Si for different diffusion times. The increase of C_{Zn_s} at the surface based on Eq. (4.18) yields $k_{-2}C_I^{\mathrm{eq}}$. The parameter $D^*_{\mathrm{Zn}_i}$ is determined by fitting Eq. (4.13) to the experimental profiles. The results from 1021 °C and the four other temperatures investigated have been reported in detail in a previous paper[42] and are given by

$$k_{-2}C_I^{\mathrm{eq}} = \left(3.3\,{}^{+3.7}_{-1.7}\right) \times 10^2 \times \exp\left(-\frac{(1.03 \pm 0.09)\,\mathrm{eV}}{k_B T}\right)\ \mathrm{s}^{-1} , \quad (4.21)$$

$$D^*_{\mathrm{Zn}_i} = \left(6.4\,{}^{+5.4}_{-2.9}\right) \times 10^{-1} \times \exp\left(-\frac{(1.85 \pm 0.07)\,\mathrm{eV}}{k_B T}\right)\ \mathrm{cm}^2\,\mathrm{s}^{-1} . \quad (4.22)$$

In the following the temperature dependences of $D^*_{\mathrm{Zn}_i}$ and $k_{-2}C_I^{\mathrm{eq}}$ are taken into account for modeling Zn diffusion in dislocation-free Si. We emphasize that care has been taken to eliminate in the evaluation of these quantities any disruptive effects due to trapping of Zn by dislocations. Experimental results confirming such interaction between dislocations and Zn have been published recently.[42]

3. Diffusion into dislocation-free Si

Diffusion regimes. During diffusion of Zn into dislocation-free Si several diffusion regimes occur. The sensivity of these regimes for variations in a particular kick-out model parameter may vary considerably. For example, in the long-time regime ($\widetilde{C}_{X_i} \approx 1$) the Zn_s profile is given by the solution of Eq. (4.6) with $D^{(a)}_{\mathrm{eff}}$ according to Eq. (4.9). Long-time profiles are therefore suited to extract D_I^* only, as shown in Fig. 6. In order to illustrate the influence of the parameter $C_I^{\mathrm{eq}}/C^{\mathrm{eq}}_{\mathrm{Zn}_s}$ on the Zn_s-profile shape, solid lines in Fig. 8 represent computer simulations of $\widetilde{C}_{\mathrm{Zn}_s}$ utilizing parameters for the kick-out model consistent with the observed Zn-diffusion behavior at 1115 °C. Dashed lines result when $C_I^{\mathrm{eq}}/C^{\mathrm{eq}}_{\mathrm{Zn}_s}$ is increased by a factor of 5 keeping the other parameters fixed. For diffusion times $t \leq (k_{-2}C_I^{\mathrm{eq}})^{-1}$ the Zn_i-Zn_s exchange can only lead to a small deviation of $C_I(x)$ from the initial equilibrium concentration C_I^{eq}. In this regime an influence of $C_I^{\mathrm{eq}}/C^{\mathrm{eq}}_{\mathrm{Zn}_s}$ on Zn_s profiles is not expected. Upon continuing diffusion the formation of Zn_s will be hampered by increasing I supersaturation which depends on the existing thermal equilibrium concentration C_I^{eq}. The calculations show an intermediate regime to be most sensitive to $C_I^{\mathrm{eq}}/C^{\mathrm{eq}}_{\mathrm{Zn}_s}$ whereas after short- and long-time diffusion no dependence is observed.

To assign experimental Zn_s profiles to various diffusion regimes, the increase of C_{Zn_s} in the center of the sample can be considered as criterion. Based on Fig. 6, profiles for which $\widetilde{C}_{Zn_s}$ at $x = d/2$ follow Eq. (4.10) are attributed to the long-time regime suitable to extract D_I^*. On the other hand, profiles whose concentration in the center deviates from Eq. (4.10) belong to the intermedi-

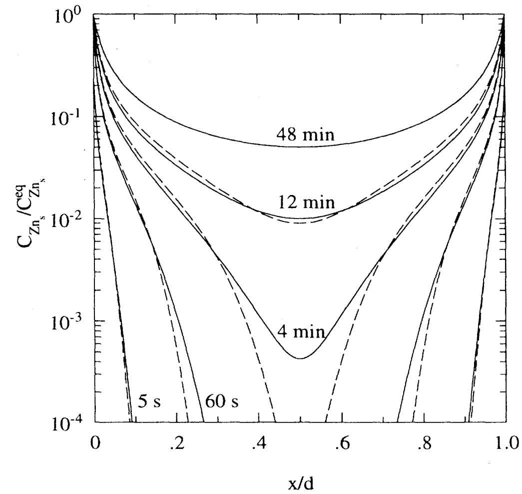

FIG. 8. Computer simulations of $\widetilde{C}_{X_s}$ in dislocation-free (ρ_d=0) Si samples (d=1500 μm) based on the kick-out model. Solid lines: $D^*_{X_i} = 1.25 \times 10^{-7}$ cm^2 s^{-1}, $D_I^* = 5.0 \times 10^{-9}$ cm^2 s^{-1}, $k_{-2}C_I^{\mathrm{eq}} = 0.059$ s^{-1}, $C^{\mathrm{eq}}_{X_i}/C^{\mathrm{eq}}_{X_s} = 1.95 \times 10^{-2}$, $C_I^{\mathrm{eq}}/C^{\mathrm{eq}}_{X_s} = 3.5 \times 10^{-4}$. Dashed lines: parameters chosen as above with $C_I^{\mathrm{eq}}/C^{\mathrm{eq}}_{X_s} = 1.75 \times 10^{-3}$.

ate stage which is most sensitive to $C_I^{eq}/C_{Zn_s}^{eq}$. Finally, profiles obtained after diffusion times so short that no Zn_s is detectable in the center of the sample are suited to determine $C_{Zn_i}^{eq}/C_{Zn_s}^{eq}$. Therefore, short-, intermediate-, and long-time experiments on dislocation-free samples yield maximum information about the above three parameters. For complete modeling of Zn diffusion in Si $k_{-2}C_I^{eq}$ and $D_{Zn_i}^*$ are taken from highly dislocated Si.

Fitting of high temperature profiles. The PDE system (4.1)–(4.3) was solved numerically. Comparison of experimental and calculated $\widetilde{C}_{Zn_s}(x,t)$ yield the parameters D_I^*, $C_I^{eq}/C_{Zn_s}^{eq}$, and $C_{Zn_i}^{eq}/C_{Zn_s}^{eq}$. Since several profiles for each diffusion regime exist, parameter values together with their statistical error are obtained.

The solid lines in Figs. 4(a)–4(c) reflect successful numerical fitting of experimental profiles measured after Zn diffusion at 1208, 1115, and 1021 °C. Notably, all experimental profiles are reproduced within the framework of the kick-out mechanism by five parameters with two of them already obtained from Zn_s profiles in highly dislocated Si. After fitting, the corresponding distributions of Zn_i and I emerge from the computer calculations. Figure 9 displays how the I supersaturation develops with increasing duration of annealing at 1115 °C. Since excess self-interstitials produced by the kick-out reaction can disappear at the surface as well as move deeper into the sample, $\widetilde{C}_I$ maxima appear near opposite surfaces of the Si slice. These maxima shift towards the center as diffusion continues until they merge to a single maximum constituting the highest I supersaturation during the whole process. From now on generation of new self-interstitials by reaction (2.4) cannot keep up with their removal at the surfaces. Hence the supersaturation decays. Focusing on $\widetilde{C}_I$, the short-time diffusion regime is characterized by I injection into the crystal whereas the long-time regime is governed by I out-diffusion. The intermediate diffusion regime applies to I profiles, which start to merge until the maximum supersaturation is reached.

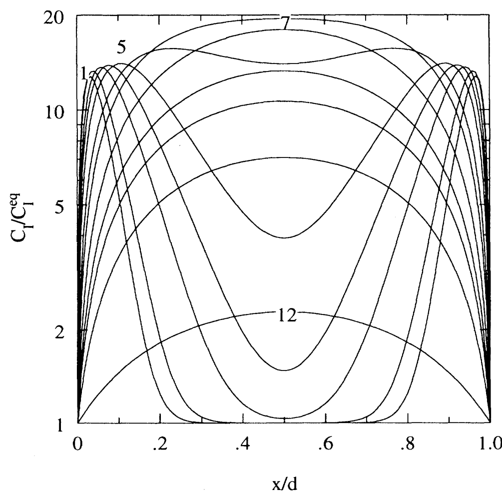

FIG. 9. Self-interstitial supersaturations $\widetilde{C}_I$ associated with the Zn_s distributions in dislocation-free Si at 1115 °C [cf. corresponding numbers in Fig. 4(b)].

TABLE III. I- and V-related parameters extracted from experimental Zn_s diffusion profiles in dislocation-free Si.

T (°C)	$\frac{C_I^{eq}}{C_{Zn_s}^{eq}}$	D_V^* (cm^2 s^{-1})	$\frac{C_V^{eq}}{C_{Zn_s}^{eq}}$
870	$(5.0\pm4.0)\times10^{-5}$	$(1.2\pm0.2)\times10^{-10}$	$(3.0\pm0.6)\times10^{-1}$
942	$(7.4\pm4.0)\times10^{-5}$	$(3.0\pm0.6)\times10^{-10}$	$(2.3\pm0.9)\times10^{-1}$
1021	$(1.0\pm0.5)\times10^{-4}$		
1115	$(3.5\pm1.5)\times10^{-4}$		
1208	$(4.2\pm2.2)\times10^{-4}$		

Fitting of low temperature profiles. In contrast to high temperatures, at 942 and 870 °C the theoretical profiles calculated on the basis of the kick-out model systematically deviate from the measured profiles. However, this deviation only appears after long-time diffusion. Profiles within $t \leq 7.2$ h at 942 °C and $t \leq 40.0$ h at 870 °C are still completely fitted by the kick-out mechanism alone.[49] Furthermore, the obtained parameter values are consistent with data extrapolated from the high temperature results. Therefore, the deviation for long-time diffusion appears reliable and is attributed to a contribution of vacancies via the dissociative mechanism [Eq. (2.5)]. Taking into account reaction (2.5), the PDE system (4.1)–(4.3) is extended by one partial differential equation which contains parameters as $D_V^*=C_V^{eq}D_V/C_{Zn_s}^{eq}$, $C_V^{eq}/C_{Zn_s}^{eq}$, and $k_{-1}C_O$, additionally.[43] k_{-1} is the reverse rate constant of reaction (2.5). Since we have found that Zn diffusion in Si is described by the kick-out model especially at the shortest diffusion times, the relationship

$$k_{-1}C_O \ll k_{-2}C_I^{eq} \tag{4.23}$$

must hold. Including the dissociative mechanism with account of Eq. (4.23), all Zn_s profiles at 942 and 870 °C are completely described also at long diffusion times as illustrated in Figs. 5(c) and 5(d), respectively. The boundary condition for V was chosen as $\widetilde{C}_V(0,t)=\widetilde{C}_V(d,t)=1$ representing an ideal source of V at the surfaces. Successful fitting, however, requires an initial vacancy concentration of $\widetilde{C}_V(x,0)\leq10^{-4}$ although a preanneal of several hours (3 h for diffusion at 942 °C and 4 h at 870 °C) was carried out to establish intrinsic point defect equilibrium. As confirmed later on by our results concerning D_V, the preanneal phase was not sufficient to establish $\widetilde{C}_V=1$ by V diffusion. Therefore, this result gives evidence that V generation in Si via the Frenkel process $I + V \rightleftharpoons 0$ is hampered.

I- and V-related model parameters extracted from the time-evolution of Zn_s profiles obtained after diffusion experiments between 1208 and 870 °C are listed in Tables II and III. The temperature dependence of the Zn-related parameter $C_{Zn_i}^{eq}/C_{Zn_s}^{eq}$ as well as other properties concerning Zn in Si will be published elsewhere.[50]

V. PROPERTIES OF INTRINSIC POINT DEFECTS

A. Transport capacities

In order to deduce the properties of intrinsic point defects from the extracted model parameters the equilib-

rium concentration $C_{\mathrm{Zn}_s}^{\mathrm{eq}}$ has to be determined as accurately as possible. Therefore, neutron activation analysis (NAA) of Si samples diffused homogeneous with Zn using an elemental Zn source were performed yielding the solubility of Zn in Si with an incertainity of 30%.[28] Assuming ideal dissolution of Zn in Si, the temperature dependence of the solubility data between 1200 and 1000 °C was successfully fitted by

$$C_{\mathrm{Zn}}^{\mathrm{eq}} = C_{\mathrm{O}} \exp\left(-\frac{G_{Zn}^{s,l}}{k_B T}\right)\left[1-\exp\left(-\frac{G_{\mathrm{Si}}^{m}}{k_B T}\right)\right] . \quad (5.1)$$

$G_{\mathrm{Zn}}^{s,l}$ is the free enthalpy of dissolution of Zn in Si, G_{Si}^{m} the free enthalpy of fusion, and k_B the Boltzmann constant. Fitting yields $H_{\mathrm{Zn}}^{s,l}$=2.49 eV and $S_{\mathrm{Zn}}^{s,l}$=7.26 k_B taking enthalpy and entropy of fusion as H_{Si}^{m}=0.525 eV and S_{Si}^{m}=3.62 k_B and a melting temperature of T_m =1412 °C.[25] In agreement with $C_{\mathrm{Zn}_i}^{\mathrm{eq}}/C_{\mathrm{Zn}_s}^{\mathrm{eq}} \lesssim 0.01$ resulting from our Zn-diffusion analysis,[50] we have $C_{\mathrm{Zn}}^{\mathrm{eq}} = C_{\mathrm{Zn}_s}^{\mathrm{eq}} + C_{\mathrm{Zn}_i}^{\mathrm{eq}} \approx C_{\mathrm{Zn}_s}^{\mathrm{eq}}$. Extrapolating the NAA results to 942 and 870 °C using Eq. (5.1), the transport capacities $C_I^{\mathrm{eq}} D_I$ and $C_V^{\mathrm{eq}} D_V$ are deduced as $C_{\mathrm{Zn}}^{\mathrm{eq}} D_I^*$ and $C_{\mathrm{Zn}}^{\mathrm{eq}} D_V^*$. We feel that this extrapolation is more reliable than taking $C_{\mathrm{Zn}_s}(x=0)$ obtained by SR analysis as estimate for $C_{\mathrm{Zn}_s}^{\mathrm{eq}}$. Transport capacities so obtained are listed in Table IV. Taking into account the qualitative result of Morehead *et al.*[51] based on Au diffusion experiments[44,52] that $C_V^{\mathrm{eq}} D_V$ equals $C_I^{\mathrm{eq}} D_I$ at 1000 °C combined with the presently determined magnitude, the temperature dependence of our data between 1208 and 870 °C is given by

$$\frac{1}{C_{\mathrm{O}}} C_I^{\mathrm{eq}} D_I = \left(3.0\,^{+1.0}_{-0.8}\right) \times 10^{3} \times \exp\left(-\frac{(4.95 \pm 0.03)\ \mathrm{eV}}{k_B T}\right) \mathrm{cm}^2\,\mathrm{s}^{-1} , \quad (5.2)$$

$$\frac{1}{C_{\mathrm{O}}} C_V^{\mathrm{eq}} D_V = \left(8.6\,^{+9.9}_{-4.6}\right) \times 10^{-2} \times \exp\left(-\frac{(3.80 \pm 0.08)\ \mathrm{eV}}{k_B T}\right) \mathrm{cm}^2\,\mathrm{s}^{-1} . \quad (5.3)$$

Figure 10 displays our results in comparison to literature data deduced from diffusion experiments with Au (Refs. 44 and 51–54) and Pt.[27,45] Data of $C_V^{\mathrm{eq}} D_V$ evaluated by Frank *et al.*[17] from diffusion experiments with Ni,[55,56] which is suggested to diffuse via the dissociative mechanism, are also included. Although different foreign atoms were used in the experiments, the resulting I- and V-related transport capacities are mutually consistent. This agreement confirms that the diffusion of these foreign atoms in Si involves interstitial-substitutional exchange. From simulations of B, P, and Au profiles Mathiot[57] deduced an Arrhenius equation for $C_V^{\mathrm{eq}} D_V$ which yields, e.g., at 942 °C a value smaller by a factor of 7 compared to Eq. (5.3). The reason for this discrepancy remains unsolved.

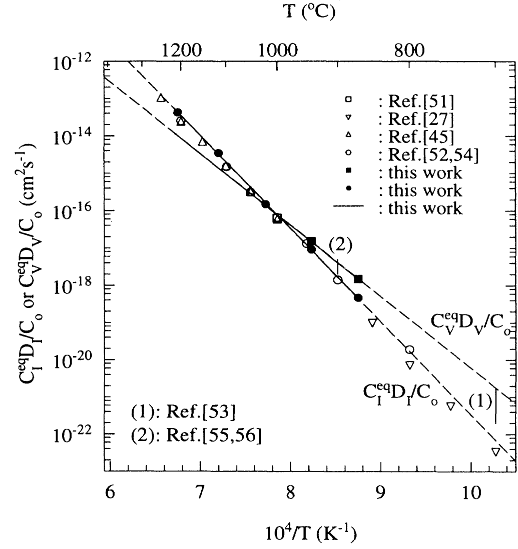

FIG. 10. Temperature dependence of transport capacities $C_I^{\mathrm{eq}} D_I$ and $C_V^{\mathrm{eq}} D_V$ in comparison to literature data.

The Arrhenius equations (5.2) and (5.3) correspond to activation enthalpies for I- and V-mediated self-diffusion of H_I^{SD}=(4.95±0.03) eV and H_V^{SD}=(3.80±0.08) eV and to activation entropies of S_I^{SD}=(13.2±0.3) k_B and S_V^{SD}=(3.4±0.8) k_B. Based on these results self-diffusion below 1000 °C is mainly governed by vacancies whereas above this temperature self-interstitials dominate. These activation enthalpies are supported by Si self-diffusion studies yielding activation enthalpies of 5 eV and 4 eV at temperatures near the melting point and far below, respectively. A comparison of Eqs. (5.2) and (5.3) with Si tracer self-diffusion coefficients D_{Si}^{T} applying Eq. (2.1) with D_{exchange}=0 is illustrated in Fig. 11. Our data are in excellent agreement with self-diffusion data of Fairfield

TABLE IV. Transport capacities and thermal equilibrium concentrations of I and V in Si deduced from Tables II and III taking into account the solubility of Zn in Si [see Eq. (5.1)].

T(°C)	$\frac{1}{C_o} C_I^{\mathrm{eq}} D_I$ (cm^2 s^{-1})	$\frac{1}{C_o} C_V^{\mathrm{eq}} D_V$ (cm^2 s^{-1})	C_I^{eq} (cm^{-3})	C_V^{eq} (cm^{-3})
870	(4.6±0.4)×10^{-19}	(1.5±0.2)×10^{-18}	(3.1±2.4)×10^{10}	(1.8±0.4)×10^{14}
942	(9.0±0.5)×10^{-18}	(1.5±0.3)×10^{-17}	(1.9±1.0)×10^{11}	(5.8±2.3)×10^{14}
1021	(1.5±0.1)×10^{-16}		(9.5±4.7)×10^{11}	
1115	(3.5±0.1)×10^{-15}		(1.2±0.5)×10^{13}	
1208	(4.3±0.2)×10^{-14}		(3.9±2.0)×10^{13}	

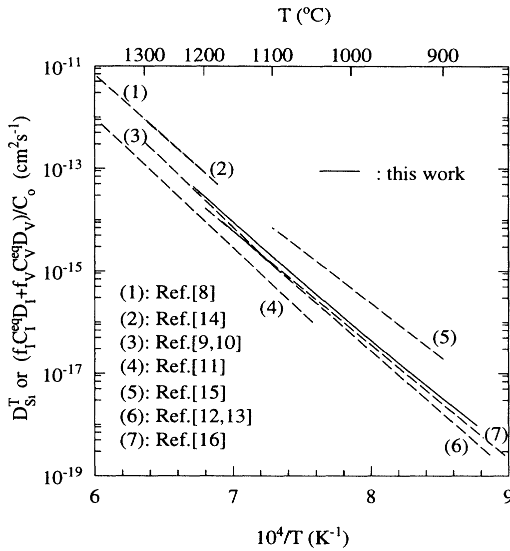

FIG. 11. Temperature dependence of Si-tracer self-diffusion coefficients $D_{\rm Si}^T$ compared to $f_I C_I^{\rm eq} D_I + f_V C_V^{\rm eq} D_V$ deduced from Zn-diffusion analysis in Si.

and Master[9,10] as well as Demond *et al.*[16] and also compatible within 50% with results given by Kalinowski and Seguin.[12,13] $D_{\rm Si}^T$ data from other authors[8,11,14,15] deviate even if one takes lower values for f_I. However, it seems difficult to conceive of microscopic I-mediated atomic exchange sequences which justify $f_I \lesssim 0.5$. Varying $D_{\rm Si}^T$ results after self-diffusion analysis using ^{31}Si (Refs. 8 and 11) may be attributed to experimental difficulties associated with this short-lived tracer atom. Deviations between the results of Hirvonen and Anttila[15] and Demond *et al.*[16] who both applied the nuclear (p,γ)-reaction technique are attributed to defects induced prior to the diffusion anneal by implantation of the natural isotope ^{30}Si serving as tracer atom. Because only Demond *et al.* recovered their Si samples prior to diffusion, their data are considered to be more reliable. Regarding the data of Ghoshtagore[14] based on experiments with ^{30}Si it remains questionable whether the natural background of ^{30}Si was substracted properly.[17] All these difficulties are avoided using ^{71}Ge with a half life-time of 11.2 days as probe for Si. Hettich *et al.*[58] performed Ge-diffusion experiments in Si and reported an activation enthalpy of 4.97 eV and 3.93 eV at temperatures above and below 1000 °C, respectively. Their results are in remarkable agreement with the activation enthalpies of I- and V-related self-diffusion deduced from our Zn-diffusion study. In addition, the Ge-diffusion coefficients given by these authors agree in magnitude with the present Si self-diffusion data. These consistencies show the usefulness of Ge as a probe for Si self-diffusion.

Our investigation of Zn diffusion in Si shows self-diffusion to occur mainly via both the interstitialcy and the vacancy mechanism (see Fig. 11). The present results supports the correlation factor $f_I \approx 0.73$ calculated by Compaan and Haven[20] for the interstitialcy mechanism. In contrast, previous comparisons between $C_I^{\rm eq} D_I$ deduced from, e.g., Au profiles and $D_{\rm Si}^T$ utilized $f_I = 0.5$,[26,52,54] however, without justification. In light of the present findings there is no reason to take another f_I value than 0.73 reliably evaluated by Compaan and Haven. Finally, the remarkable agreement between self-diffusion data obtained by Si tracer and foreign-atom studies shows the direct exchange not to play a significant role.

B. Thermal equilibrium concentrations and diffusion coefficients

Thermal equilibrium concentrations of intrinsic point defects like I and V are given by

$$C_{I,V}^{\rm eq} = C_0 \exp\left(-\frac{G_{I,V}^F}{k_B T}\right) , \qquad (5.4)$$

where $G_{I,V}^F = H_{I,V}^F - T S_{I,V}^F$ is the free enthalpy of formation with $H_{I,V}^F$ and $S_{I,V}^F$ the enthalpy and entropy of formation, respectively. In case of cubic crystals, the diffusion coefficients $D_{I,V}$ can be written as

$$D_{I,V} = g_{I,V}\, a_0^2\, \nu_{I0,V0} \exp\left(-\frac{G_{I,V}^M}{k_B T}\right) , \qquad (5.5)$$

where $G_{I,V}^M (= H_{I,V}^M - T S_{I,V}^M)$ is the free enthalpy of migration. The geometry factor $g_{I,V}$ depends on the crystal structure and on the microscopic jump geometry of the diffusion process. The factor a_0 is the Si lattice constant (5.431×10^{-10} m) and $\nu_{I0,V0}$ are attempt frequencies. Assuming a periodic lattice potential which is harmonic at the Si-lattice sites, these frequencies can be estimated as

$$\nu_{I0,V0} = \frac{2}{a_0}\left(\frac{2 H_{I,V}^M}{3 m_{\rm Si}}\right)^{0.5} , \qquad (5.6)$$

where $m_{\rm Si}$ is the mass of an Si atom. For I- and V-mediated self-diffusion via the interstitialcy or the vacancy mechanism, the geometry factors are given by $g_I = 1/4$ (Ref. 59) or $g_V = 1/8$.[60]

1. *Si self-interstitials*

Thermal equilibrium concentrations of Si self-interstitials $C_I^{\rm eq}$ given by combining Eq. (5.1) and the extracted model parameter $C_I^{\rm eq}/C_{\rm Zn_s}^{\rm eq}$ summarized in Table III are listed in Table IV. The temperature dependences of $C_I^{\rm eq} = (C_I^{\rm eq}/C_{\rm Zn_s}^{\rm eq}) \times C_{\rm Zn}^{\rm eq}$ and $D_I = D_I^*/(C_I^{\rm eq}/C_{\rm Zn_s}^{\rm eq})$ are described by

$$C_I^{\rm eq} = \left(2.9\,^{+8.2}_{-2.1}\right) \times 10^{24} \times \exp\left(-\frac{(3.18 \pm 0.15)\ {\rm eV}}{k_B T}\right)\ {\rm cm}^{-3} , \qquad (5.7)$$

$$D_I = \left(5.1\,^{+9.4}_{-3.3}\right) \times 10^{1} \times \exp\left(-\frac{(1.77 \pm 0.12)\ {\rm eV}}{k_B T}\right)\ {\rm cm}^2\,{\rm s}^{-1} . \qquad (5.8)$$

These equations involve a formation enthalpy $H_I^F = (3.18 \pm 0.15)$ eV and a migration enthalpy $H_I^M = (1.77 \pm 0.12)$ eV for Si self-interstitials. The entropy data result as $S_I^F = (4.1 \pm 1.3)\, k_B$ and $S_I^M = (9.1 \pm 1.0)\, k_B$ taking into account Eq. (5.6).

2. Vacancies

In order to deduce the thermodynamic and transport properties of vacancies in Si, we consider the temperature dependence of the transport capacity $C_V^{\rm eq} D_V$ to be more reliable than that of $C_V^{\rm eq}$ and D_V, which each rely on two data points only. Fitting an Arrhenius equation to our $C_V^{\rm eq}$ data yields

$$C_V^{\rm eq} \approx 1.4 \times 10^{23} \exp\left(-\frac{2.0\,{\rm eV}}{k_B T}\right)\ {\rm cm}^{-3} \qquad (5.9)$$

assuming a vacancy formation entropy of $S_V^F = 1k_B$. Without this restriction a slightly negative value would result for S_V^F. A vacancy formation enthalpy H_V^F of about 2 eV is given by Eq. (5.9). According to Eq. (5.3) the activation enthalpy of V-mediated self-diffusion $H_V^{\rm SD} = H_V^F + H_V^M$ is 3.80 eV. Therefore 1.8 eV remains as vacancy migration enthalpy H_V^M. The entropy of V-mediated self-diffusion $S_V^{\rm SD} = S_V^F + S_V^M = (3.4 \pm 0.8) k_B$ was calculated from the preexponential factor of Eq. (5.3) taking into account Eq. (5.6). With $S_V^F = 1k_B$, the migration entropy S_V^M is nearly $2.4 k_B$. Based on these data the temperature dependence of D_V is given by

$$D_V \approx 3.0 \times 10^{-2} \exp\left(-\frac{1.8\,{\rm eV}}{k_B T}\right)\ {\rm cm}^2\,{\rm s}^{-1}. \qquad (5.10)$$

C. Discussion

Equilibrium concentrations $C_I^{\rm eq}$ and diffusion coefficients D_I determined from our present Zn-diffusion study are displayed by Figs. 12(a) and 13(a), respectively. The dashed lines represent previous experimental estimates. They are deduced from Au and Pt diffusion into dislocation-free Si,[61–64] investigations involving oxidation processes,[65–67] crystal growth studies,[68] and estimates taking into account the interstitial nature of A-type swirl defects.[69] The temperature dependences of $C_I^{\rm eq}$ and D_I given by Morehead[61] and Zimmermann *et al.*[62] are fully or mainly based on reanalyses of Au- and Pt-diffusion profiles originally reported by other investigators.[27,44,45,52] Moreover, both studies[61,62] make explicit use of the $C_I^{\rm eq} D_I$ data extracted by Stolwijk *et al.*[44,52] from Au diffusion experiments. We emphasize that the Au and Pt profiles analyzed belong mainly (Au) or entirely (Pt) to the long-time diffusion regime. This becomes obvious from the observation that the profiles used for those analyses of $C_I^{\rm eq}$ and D_I (Refs. 61 and 62) either fulfill Eq. (4.10) (see Refs. 44, 52, 54, and 62) or are well described by Eq. (4.6) on the basis of the long-time diffusivity D_I^* in Eq. (4.9) (see Ref. 27). Therefore the Au and Pt profiles analyzed by Morehead and Zimmermann are expected to be not as sensitive to $C_I^{\rm eq}$ (and D_I) as the concentration profiles of Zn given in the present paper. Boit *et al.*[63] and recently Ghaderi *et al.*[64] have investigated diffusion profiles of Au obtained after short annealing times. Data of $C_I^{\rm eq}$ and D_I given by these authors are not consistent among themselves and also deviate from our results. This deviation may be attributed to uncertainties in performing short-time isothermal diffusion with commercial rapid thermal annealing systems (steep heating ramp, inaccurate temperature measurement) or to the lack of Au profiles belonging to the intermediate diffusion regime particulary sensitive to $C_I^{\rm eq}$. Especially, the analysis of Au-diffusion profiles by Ghaderi *et al.* seems to be questionable. They report an activa-

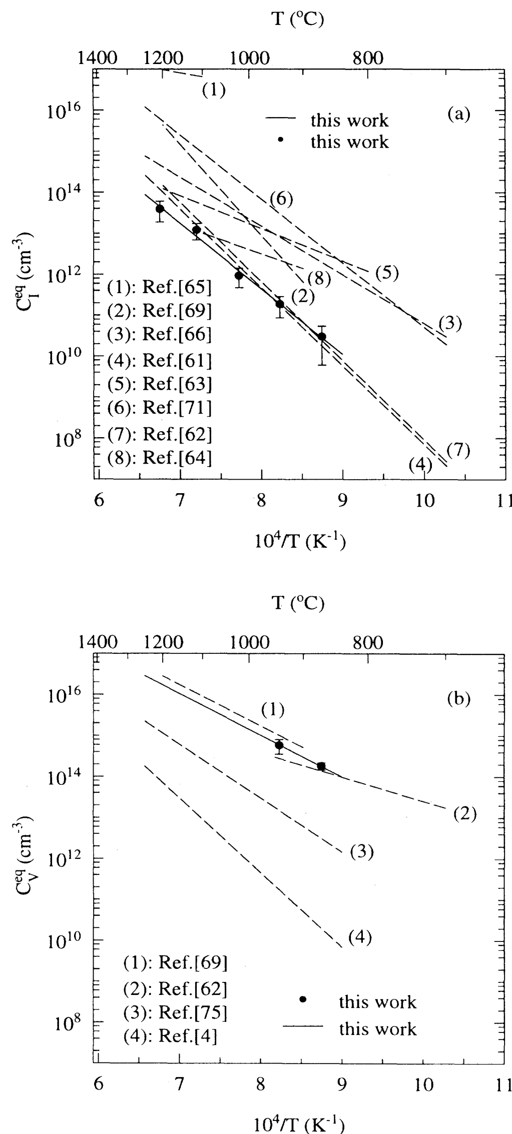

FIG. 12. Temperature dependence of (a) $C_I^{\rm eq}$ and (b) $C_V^{\rm eq}$ in comparison to literature data.

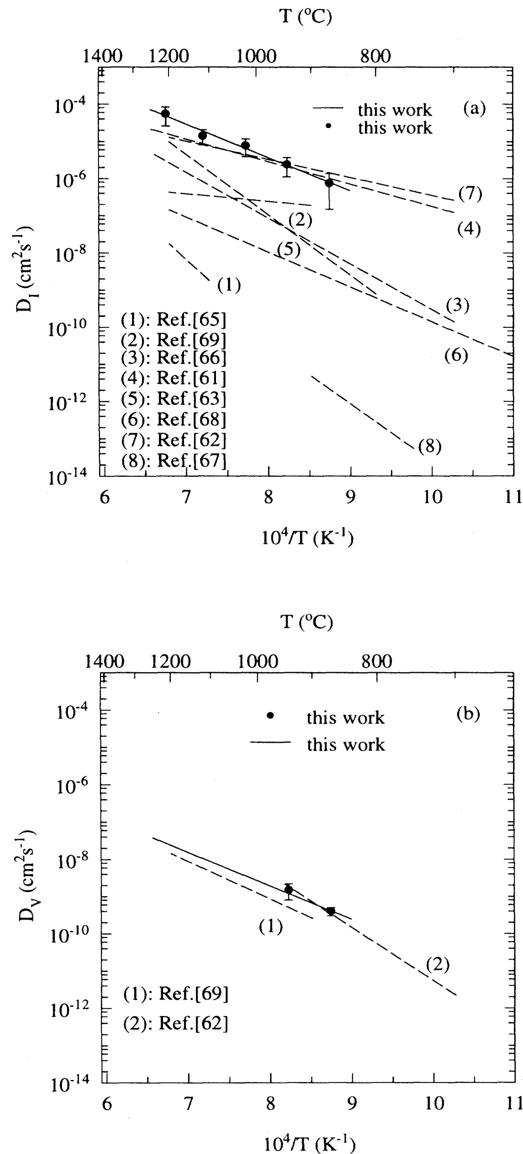

FIG. 13. Temperature dependence of (a) D_I and (b) D_V in comparison to literature data.

tion enthalpy of $H_I^{\rm SD}=5.8$ eV in contradiction with the results of self-diffusion studies yielding values in the range of 4–5 eV.[17]

It has been established that thermal oxidation of Si surface injects self-interstitials. Such injection processes were performed, e.g., by Taniguchi *et al.*[65] and Griffin *et al.*[70] in order to extract information about Si self-interstitials from oxidation induced stacking faults and oxidation enhanced and retarded diffusion of dopants, respectively. Griffin *et al.* reported for the self-interstitial diffusivity $D_I \approx 2 \times 10^{-7}$ cm^2 s^{-1} at 1200 °C. The authors considered their data as lower bounds, which is consistent with the present result. Wijaranakula[68,71] used the formation of oxygen thermal donors at temperatures of about 500 °C to gain information about self-interstitials. Assuming the model of oxygen donor formation as proposed by Ourmazd *et al.*,[24] Wijaranakula deduced $H_I^m=1.86$ eV taking into account the data of Griffin, additionally. Whereas the extracted migration enthalpy is consistent with our results, his absolute diffusivities are several orders of magnitudes lower than the present ones. In agreement with our results, Yamanaka and Aoki[72] deduced $D_I=5.9\times10^{-6}$ cm^2 s^{-1} from the depth profiles of oxygen precipitates in Si samples after heat treatments at 1000 °C in an oxidizing ambient. Gossmann *et al.*[67] investigated the broadening of periodically arranged boron spikes grown by molecular beam epitaxy (MBE) during dry oxidation and extracted D_I data being more than five orders of decades lower than our data. Given the well established value of $C_I^{\rm eq}D_I$, $C_I^{\rm eq}$ values result which exceed the solubility of Au or Zn in Si considerably. In that case, however, I-controlled diffusion of Au or Zn in dislocation-free Si which requires Eq. (2.6) to be valid would not occur, in contrast with the experimental observations. In general, data based on oxidation processes give no consistent results. Presumably, these processes are too complex and not yet sufficiently understood for detailed modeling.

In a recent paper Stolk *et al.*[73] gave experimental evidence that the diffusion of self-interstitials in Si grown by MBE is limited by trapping at impurities and show that the low D_I value given by Gossmann *et al.* is explained within this model. A more detailed experimental study[74] supports that substitutional carbon is the dominant impurity reponsible for the occurrence of I trapping. The carbon and oxygen concentration of the high-Ohmic Si used were 2×10^{16} cm^{-3} and 1.4×10^{15} cm^{-3}, respectively. A possible influence of carbon was checked by additional experiments of Zn diffusion into FZ-Si with a carbon concentration of 5×10^{14} cm^{-3}. The profiles measured with the SR technique are completely described on the basis of the kick-out model using the parameter set given in the present paper. Therefore, we believe that the Zn_s profiles analyzed above are not significantly affected by substitutional carbon.

Results concerning $C_I^{\rm eq}$ given by Bronner and Plummer[66] are extracted from enhanced phosphorus diffusion and extrinsic gettering of gold at 700 and 800 °C. The deviation of their data from our results remains unclear and possibly shows that the mechanism of gettering is not only limited by the diffusion of self-interstitials as assumed in their analysis. It should be noted that literature data of $C_I^{\rm eq}$ significantly exceeding our values conflict with the observed Zn-diffusion behavior. This is illustrated in Fig. 8 by the kick-out profiles calculated by using model parameters describing the Zn profiles measured at 1115 °C (solid lines). For $C_I^{\rm eq}$ larger by a factor of 5 (or more) than obtained from the Zn-diffusion analysis different profiles would result (dashed lines) particularly at intermediate diffusion times. The present Zn concentration profiles covering all diffusion regimes (from short to long times) enable a reliable extraction of the thermodynamic and transport properties especially of Si self-interstitials. Diffusion profiles of Au and Pt in Si were also frequently used to calculate these properties but most of these profiles already belong to

the long-time diffusion regime. On closer inspection $C_I^{\rm eq}$ data previously deduced from such Au and Pt profiles rather represent upper limits.[61,62] Accidentally, these upper limits turn out to be not far above our $C_I^{\rm eq}$ data.

The temperature dependence of our $C_V^{\rm eq}$ and D_V data is displayed in Figs. 12(b) and 13(b), respectively. Figure 12(b) also includes results obtained from positron annihilation experiments carried out by Dannefaer *et al.*[4] yielding a vacancy formation enthalpy of H_V^F=3.6 eV. The same positron annihilation data were analyzed by Van Vechten[75] leading to H_V^F=2.4 eV. In contrast to Dannefaer, Van Vechten proposed simultaneous contribution of mono- and divacancies to the mean positron lifetime rather than monovacancies alone. However, positron annihilation studies performed by Würschum *et al.*[5] show no reliable correlation of the positron lifetime with vacancies, which is interpreted by them in terms of vacancy concentrations too low to be detected by positrons. Therefore, the vacancy formation enthalpies given by Dannefaer *et al.* and Van Vechten may be questionable. Zimmermann and Ryssel[62] performed experiments with Pt and reported diffusion between 850 and 700 °C to be governed by the dissociative diffusion mechanism. Although their $C_V^{\rm eq}$ data are of the same magnitude as the present ones, the temperature dependence given by Zimmermann implies a negative formation entropy. The corresponding temperature dependence of D_V shown in Fig. 13(b) was deduced using $C_V^{\rm eq}D_V$ reported in Ref. 69. Tan and Gösele[69] deduced an upper limit for $C_V^{\rm eq}$ from $C_{{\rm Au}_s}^{\rm eq} > C_V^{\rm eq}$ necessary for V-controlled Au diffusion. As shown in Fig. 12(b), this crude estimation is in reasonable agreement with our $C_V^{\rm eq}$ data as well as their estimation of D_V illustrated in Fig. 13(b). A strong discrepancy exists between our vacancy migration enthalpy in the high-temperature regime and the results of Watkins *et al.*[22] obtained at low temperatures, e.g., $H_V^M \sim 0.18$–0.45 eV. The reason for this discrepancy is unsolved but may indicate different structures of the vacancy at low and high temperatures.

During Si crystal growth several types of microscopic defects may be formed due to agglomeration of Si self-interstitials (A defects) or vacancies (D defects). Efforts to model crystal growth have been undertaken, e.g., by Wijaranakula[71] and Habu *et al.*[76] in order to understand the occurrence and distribution of grown-in defects in Czochralski (CZ) Si. As a result Habu *et al.* proposed the recombination of I and V to be suppressed at high temperature and facilitated at low temperature supporting an *entropy* barrier against pair annihilation rather than an *enthalpy* barrier. The ineffectiveness of Frenkel pair generation or recombination is also proposed by Zimmermann and Ryssel[62] on the basis of Pt profiles obtained after diffusion at $T \leq 850$ °C. Fitting of our experimental Zn profiles requires an initial vacancy concentration of $C_V(x,0)/C_V^{\rm eq} \leq 10^{-4}$ although an anneal of several hours prior to Zn diffusion was carried out to establish intrinsic point defect equilibrium. Consistently, the present D_V data (e.g., 1.3×10^{-9} cm^2 s^{-1} at 942 °C) show indiffusion of V from the surfaces during the preanneal phase of 3 h to be insufficient to establish $C_V(x,0)=C_V^{\rm eq}$. This finding provides evidence for a barrier to vacancy-interstitial generation.

The present work yields $C_V^{\rm eq} \simeq 100 C_I^{\rm eq}$ near the melting point. This agrees with the result from Simmons-Balluffi experiments given by Okada[6] indicating that vacancies are the dominant intrinsic point defect in FZ Si at high temperatures. However, Okada's data are widely scattered and therefore his result may remain doubtful. The dominance of vacancies conflicts with the model of A-type swirl defect formation proposed by Föll and Kolbesen.[77] Using transmission electron microscopy (TEM) these authors identified A defects as interstitial-type dislocation loops. They concluded that the A defects are formed during crystal growth by agglomeration of high-temperature equilibrium self-interstitials which remain after V-I recombination and proposed that the dominant intrinsic defect in Si is the self-interstitial. Beside A-type defects also B-type defects appear which exert only a weak strain on the lattice. For this reason among others, the nature of these defects could not be identified unambiguously hitherto.[78] Föll and Kolbesen assumed that B defects are also of interstitial type and precursors of the A defects. An alternative model of swirl defect formation suggested already several years ago by Hu is described in a recent review of this author.[79] Hu assumed that excess vacancies and self-interstitials do not annihilate completely and may agglomerate into A and B defects, separately. In his picture the larger A defects are precipitates of self-interstitials in form of dislocation loops in accordance with TEM investigations and the B defects are assumed to be agglomerates of vacancies in form of small globules.[79] Thereby the special geometry of the different precipitates causes A clusters to be detectable by TEM whereas small spherical B clusters are not as easily observable. As a consequence of this interpretation, a barrier to V-I recombination must exist which is not required by the Föll-Kolbesen model. The present analysis supports the Hu model of swirl-defect formation, since it not only shows the relationship $C_V^{\rm eq} > C_I^{\rm eq}$ to be valid near the melting point and below but also provides evidence for a V-I recombination barrier in agreement with the above mentioned result obtained by Habu *et al.*[76] Although our conclusion is based on two $C_V^{\rm eq}$ data only, the inequality $C_V^{\rm eq} > C_I^{\rm eq}$ safely holds within the statistical errors given for $C_I^{\rm eq}$ and $C_V^{\rm eq}$.

Finally our results are compared to theoretical calculations of point defects properties of Si. A recent first-principles calculation of $H_I^F \simeq (3.3 \pm 0.2)$ eV and $S_I^F \simeq (6 \pm 2)k_B$ by Blöchl *et al.*[80] is in excellent agreement with our results summarized in Table V as well as their estimate of $D_I \approx 10^{-4}$ cm^2 s^{-1} at 1500 K. However, their values for $H_V^F \simeq (4.1 \pm 0.2)$ eV and $S_V^F \simeq (5 \pm 2)k_B$ deviate from our data. Atomistic simulations of thermodynamic and transport properties of intrinsic point defects in Si were recently published by Maroudas and Brown.[81,82] Their calculations for extended self-interstitials and extended vacancies yield the formation enthalpies $H_I^F \simeq 3.67$ eV and $H_V^F \simeq 2.61$ eV, respectively, as well as the corresponding entropies $S_I^F \simeq 5.5\ k_B$ and $S_V^F \simeq 2.2\ k_B$,[82] which are in reasonable agreement with

TABLE V. Thermodynamic and transport properties of self-interstitials (I) and vacancies (V) of intrinsic Si determined by Zn-diffusion analysis compared to the results of first-principles calculations by Blöchl *et al.* (Ref. 80) and of atomistic simulations for a reference temperature of 500 °C by Maroudas and Brown (Refs. 80 and 82).

Defect	H^F (eV)	H^M (eV)	S^F (k_B)	S^M (k_B)	Reference
I	3.18±0.15	1.77±0.12	4.1±1.3	9.1±1.0	this work
V	~ 2.0	~ 1.8	~ 1	~ 2.4	this work
I	3.3±0.2		6±2		80
V	4.1±0.2		5±2		80
I	3.67±0.05	~1.7	5.5±2.2	~2.7	81,82
V	2.61±0.05	~0.48	2.2±2.2	~0.3	82

our experimental results. These results together with their data calculated for the entropy and enthalpy of migration are listed in Table V.

VI. CONCLUSIONS

Diffusion of Zn into dislocation-free and highly dislocated Si monocrystals between 1208 and 870 °C was investigated in detail showing unambiguous evidence for the predominance of the kick-out diffusion mechanism. All concentration profiles of Zn measured with the help of spreading-resistance analysis after short-, intermediate-, and long-time diffusion experiments are completely fitted by numerical solutions based on the kick-out mechanism alone at high T and an additional contribution of the dissociative diffusion mechanism at low T. Profiles belonging to different diffusion regimes are indispensable to gain maximum information about intrinsic point-defect properties. Especially, the shape of the Zn profile after intermediate times is strongly affected by the thermal equilibrium concentration of Si self-interstitials. Results obtained for thermodynamic and transport properties of intrinsic point defects in Si are summarized in Table V. Fitting experimental Zn profiles provides evidence for a barrier to vacancy-interstitial generation. Our finding that vacancies are more abundant than self-interstitials even near the Si melting point supports the model of swirl defect formation proposed by Hu.[79] Analysis of Zn diffusion in Si shows Si self-diffusion to be governed by the interstitialcy mechanism above 1000 °C, whereas below this temperature the vacancy mechanism dominates. Comparison of the present results with the theoretical calculations of Blöchl *et al.*[80] and Maroudas and Brown[81,82] reveals satisfactory agreement between experiment and theory for many point-defect properties of Si.

ACKNOWLEDGMENTS

We thank Dr. I. Yonenaga (Tohoku University, Sendai) and Dr. V. Lehmann (Siemens AG, München) for donating highly dislocated and dislocation-free Si, respectively, as well as Dr. W. Zulchner for determining the oxygen and carbon concentration of the high-Ohmic Si used. Financial support by the "Deutsche Forschungsgemeinschaft" is gratefully acknowledged.

[1] A.C. Damask and G.J. Dienes, *Point Defects in Metals* (Gordon and Breach, New York, 1963).
[2] L.C. Smedskjaer and M.J. Fluss, in *Methods of Experimental Physics, Vol. 21, Nuclear Methods*, edited by J.N. Mundy, S.J. Rothmann, M.J. Fluss, and L.C. Smedskjaer (Academic Press, Orlando, 1983), p. 77.
[3] R.O. Simmons and R.W. Balluffi, Phys. Rev. **117**, 52 (1960).
[4] S. Dannefaer, P. Mascher, and D. Kerr, Phys. Rev. Lett. **56**, 2195 (1986).
[5] R. Würschum, W. Bauer, K. Maier, A. Seeger, and H.-E. Schaefer, J. Phys. Condens. Matter **1**, SA33 (1989).
[6] Y. Okada, Phys. Rev. B **41**, 10 741 (1990).
[7] P.M. Fahey, P.B. Griffin, and J.D. Plummer, Rev. Mod. Phys. **61**, 289 (1989).
[8] R.F. Peart, Phys. Status Solidi **15**, K119 (1966).
[9] B.J. Masters and J.M. Fairfield, Appl. Phys. Lett. **8**, 280 (1966).
[10] J.M. Fairfield and B.J. Masters, J. Appl. Phys. **38**, 3148 (1967).
[11] H.J. Mayer, H. Mehrer, and K. Maier, *Radiation Effects in Semiconductors 1976*, IOP Conf. Proc. No. 31 (Institute of Physics, London, 1977), p. 186.
[12] L. Kalinowski and R. Seguin, Appl. Phys. Lett. **35**, 211 (1979).
[13] L. Kalinowski and R. Seguin, Appl. Phys. Lett. **36**, 171 (1980).
[14] R.N. Ghoshtagore, Phys. Rev. Lett. **16**, 890 (1966).
[15] J. Hirvonen and A. Anttila, Appl. Phys. Lett. **35**, 703 (1979).
[16] F.J. Demond, S. Kalbitzer, H. Mannsperger, and H. Damjantschitsch, Phys. Lett. **93A**, 503 (1983).
[17] W. Frank, U. Gösele, H. Mehrer, and A. Seeger, in *Diffusion in Crystalline Solids*, edited by G.E. Murch and A.S. Nowick (Academic Press, New York, 1984).
[18] K.C. Pandey, Phys. Rev. Lett. **57**, 2287 (1986).
[19] K. Compaan and Y. Haven, Trans. Faraday Soc. **52**, 786 (1956).
[20] K. Compaan and Y. Haven, Trans. Faraday Soc. **54**, 1498 (1958).

[21] G.D. Watkins, in *Lattice Defects in Semiconductors*, edited by F.A. Huntley, IOP Conf. Proc. No. 23 (Institute of Physics and Physical Society, London, 1975), p. 1.
[22] G.D. Watkins, J.R. Troxell, and A.P. Chatterjee, in *Defects and Radiation Effects in Semiconductors*, edited by J.H. Albany, IOP Conf. Proc. No. 46 (Institute of Physics and Physical Society, London, 1979), p. 16.
[23] G.D. Watkins and J.R. Troxell, Phys. Rev. Lett. **44**, 593 (1980).
[24] A. Ourmazd, W. Schröter, and A. Bourret, J. Appl. Phys. **56**, 1670 (1984).
[25] E.R. Weber, Appl. Phys. A **33**, 1 (1983).
[26] U. Gösele, W. Frank, and A. Seeger, Appl. Phys. **23**, 361 (1980).
[27] S. Mantovani, F. Nava, S. Nobili, and G. Ottaviani, Phys. Rev. B **33**, 5536 (1986).
[28] D. Grünebaum, Th. Czekalla, N.A. Stolwijk, H. Mehrer, I. Yonenaga, and K. Sumino, Appl. Phys. A **53**, 65 (1991).
[29] W. Kern and D.A. Puotinen, RCA Rev. **31**, 187 (1970).
[30] S.J. Nelson, in *Selected Values of the Thermodynamic Properties of the Elements*, prepared by R. Hultgren, P.D. Desai, D.T. Hawkins, M. Gleiser, K.K. Kelley, and D.D. Wagman (American Society for Metals, Metals Park, OH, 1973), p. 565.
[31] H. Bracht, N.A. Stolwijk, H. Mehrer, and I. Yonenaga, Appl. Phys. Lett. **59**, 3559 (1991).
[32] J.M. Herman and C.T. Sah, Phys. Status Solidi A **14**, 405 (1972).
[33] A. Dörnen, R. Kienle, K. Thonke, P. Stolz, G. Pensl, D. Grünebaum, and N.A. Stolwijk, Phys. Rev. B **40**, 12 005 (1989).
[34] E. Merk, J. Heyman, and E.E. Haller, Solid State Commun. **72**, 851 (1989).
[35] P. Stolz, doctoral thesis, University of Erlangen, 1990.
[36] P. Stolz, G. Pensl, D. Grünebaum, and N.A. Stolwijk, Mater. Sci. Eng. **B4**, 31 (1989).
[37] R.O. Carlson, Phys. Rev. **108**, 1390 (1957).
[38] H. Lemke, Phys. Status Solidi A **72**, 177 (1982).
[39] S. Weiss, R. Beckmann, and R. Kassing, Appl. Phys. A **50**, 151 (1990).
[40] H.E. Altink, T. Gregorkiewicz, and C.A.J. Ammerlaan, Solid State Commun. **75**, 115 (1990).
[41] M. Pawlik, J. Vac. Sci. Technol. B **10**, 388 (1992).
[42] H. Bracht, N.A. Stolwijk, I. Yonenaga, and H. Mehrer, Phys. Status Solidi A **137**, 499 (1993).
[43] H. Bracht, N.A. Stolwijk, and H. Mehrer, in *Semiconductor Silicon/1994*, edited by H.R. Huff, W. Bergholz, and K. Sumino (The Electrochemical Society, Pennington, NJ, 1994), Vol. 94-10, p. 593.
[44] N.A. Stolwijk, B. Schuster, J. Hölzl, H. Mehrer, and W. Frank, Physica B&C **116B**, 335 (1983).
[45] J. Hauber, W. Frank, and N.A. Stolwijk, Mater. Sci. Forum **38-41**, 707 (1989).
[46] W. Jüngling, P. Pichler, S. Selberherr, E. Guerrero, and H.W. Pötzl, IEEE Trans. Electron. Devices **ED-32**, 156 (1985).
[47] G.L.J. Ouwerling, doctoral thesis, Delft University of Technology, 1989.
[48] J. Hauber, N.A. Stolwijk, L. Tapfer, H. Mehrer, and W. Frank, J. Phys. C **19**, 5817 (1986).
[49] H. Bracht, doctoral thesis, University of Münster, 1993.
[50] H. Bracht (unpublished).
[51] F. Morehead, N.A. Stolwijk, W. Meyberg, and U. Gösele, Appl. Phys. Lett. **42**, 690 (1983).
[52] N.A. Stolwijk, B. Schuster, and J. Hölzl, Appl. Phys. A **33**, 133 (1984).
[53] W.R. Wilcox and T.J. LaChapelle, J. Appl. Phys. **35**, 240 (1964).
[54] N.A. Stolwijk, J. Hölzl, W. Frank, E.R. Weber, and H. Mehrer, Appl. Phys. A **39**, 37 (1986).
[55] H. Kitagawa, K. Hashimoto, and M. Yoshida, Jpn. J. Appl. Phys. **21**, 276 (1982).
[56] H. Kitagawa, K. Hashimoto, and M. Yoshida, Physica B&C **116B**, 323 (1983).
[57] D. Mathiot, Phys. Rev. B **45**, 13 345 (1992).
[58] G. Hettich, H. Mehrer, and K. Maier, in *Defects and Radiation Effects in Semiconductors* (Ref. 22), p. 500.
[59] A. Seeger, H. Föll, and W. Frank, *Radiation Effects in Semiconductors 1976* (Ref. 11), p. 12.
[60] A. Seeger and K.P. Chik, Phys. Status Solidi **29**, 455 (1968).
[61] F.F. Morehead, in *Defects in Electronic Materials*, edited by M. Stavola, S.J. Pearton, and G. Davies, MRS Symposia Proceedings No. 104 (Materials Research Society, Pittsburgh, 1988), p. 99.
[62] H. Zimmermann and H. Ryssel, Appl. Phys. A **55**, 121 (1992).
[63] C. Boit, F. Lau, and R. Sittig, Appl. Phys. A **50**, 197 (1990).
[64] K. Ghaderi, G. Hobler, M. Budil, L. Mader, and H.J. Schulze, J. Appl. Phys. **77**, 1320 (1995).
[65] K. Taniguchi, D.A. Antoniadis, and Y. Matsushita, Appl. Phys. Lett. **42**, 961 (1983).
[66] G.B. Bronner and J.D. Plummer, J. Appl. Phys. **61**, 5286 (1987).
[67] H.-J. Gossmann, C.S. Rafferty, H.S. Luftmann, F.C. Unterwald, T. Boone, and J.M. Poate, Appl. Phys. Lett. **63**, 639 (1993).
[68] W. Wijaranakula, J. Appl. Phys. **67**, 7624 (1990).
[69] T.Y. Tan and U. Gösele, Appl. Phys. A **37**, 1 (1985).
[70] P.B. Griffin, P.M. Fahey, J.D. Plummer, and R.W. Dutton, Appl. Phys. Lett. **47**, 319 (1985).
[71] W. Wijaranakula, J. Electrochem. Soc. **139**, 604 (1992).
[72] H. Yamanaka and Y. Aoki, Jpn. J. Appl. Phys. **33**, L559 (1994).
[73] P.A. Stolk, H.-J. Gossmann, D.J. Eaglesham, D.C. Jacobson, J.M. Poate, and H.S. Luftmann, Appl. Phys. Lett. **66**, 568 (1995).
[74] P.A. Stolk, D.J. Eaglesham, H.-J. Gossmann, and J.M. Poate, Appl. Phys. Lett. **66**, 1370 (1995).
[75] J.A. Van Vechten, Phys. Rev. B **33**, 2674 (1986).
[76] R. Habu, T. Iwasaki, H. Harada, and A. Tomiura, Jpn. J. Appl. Phys. **33**, 1234 (1994).
[77] H. Föll and B.O. Kolbesen, Appl. Phys. **8**, 319 (1975).
[78] *Impurities and Defects in Group IV Elements and III-V Compounds*, edited by M. Schulz, Landolt-Börnstein, New Series, Group III, Vol. 22, Pt. b (Springer, Berlin, 1989).
[79] S.M. Hu, Mater. Sci. Eng. **R13**, 105 (1994).
[80] P.E. Blöchl, E. Smargiassi, R. Car, D.B. Laks, W. Andreoni, and S.T. Pantelidis, Phys. Rev. Lett. **70**, 2435 (1993).
[81] D. Maroudas and R.A. Brown, Appl. Phys. Lett. **62**, 172 (1993).
[82] D. Maroudas and R.A. Brown, Phys. Rev. B **47**, 15 562 (1993).